

# Exploring the design space of deep-learning-based weather forecasting systems

Shoaib Ahmed Siddiqui

msas3@cam.ac.uk

University of Cambridge, UK

Jean Kossaifi

jkossaifi@nvidia.com

NVIDIA Research, USA

Boris Bonev

bbonev@nvidia.com

NVIDIA Research, Switzerland

Christopher Choy

cchoy@nvidia.com

NVIDIA Research, USA

Jan Kautz

jkautz@nvidia.com

NVIDIA Research, USA

David Krueger

dsk30@cam.ac.uk

University of Cambridge, UK

Kamyar Azizzadenesheli

kamyara@nvidia.com

NVIDIA Research, USA

## Abstract

Despite tremendous progress in developing deep-learning-based weather forecasting systems, their design space, including the impact of different design choices, is yet to be well understood. This paper aims to fill this knowledge gap by systematically analyzing these choices including architecture, problem formulation, pretraining scheme, use of image-based pretrained models, loss functions, noise injection, multi-step inputs, additional static masks, multi-step finetuning (including larger stride models), as well as training on a larger dataset. We study fixed-grid architectures such as UNet, fully convolutional architectures, and transformer-based models, along with grid-invariant architectures, including graph-based and operator-based models. Our results show that fixed-grid architectures outperform grid-invariant architectures, indicating a need for further architectural developments in grid-invariant models such as neural operators. We therefore propose a hybrid system that combines the strong performance of fixed-grid models with the flexibility of grid-invariant architectures. We further show that multi-step fine-tuning is essential for most deep-learning models to work well in practice, which has been a common practice in the past. Pretraining objectives degrade performance in comparison to supervised training, while image-based pretrained models provide useful inductive biases in some cases in comparison to training the model from scratch. Interestingly, we see a strong positive effect of using a larger dataset when training a smaller model as compared to training on a smaller dataset for longer. Larger models, on the other hand, primarily benefit from just an increase in the computational budget. We believe that these results will aid in the design of better weather forecasting systems in the future.

## 1 Introduction

Deep learning for weather forecasting has been a very active area of research in the recent past, with many newer deep-learning-based models approaching the performance of numerical weather prediction systems while being orders of magnitude faster and energy efficient (Pathak et al., 2022; Bi et al., 2022; Lam et al., 2022; Price et al., 2023). Despite these advances, the justification for the design decisions, including model architectures, is rarely described (Pathak et al., 2022; Bi et al., 2022; Lam et al., 2022; Price et al., 2023). While it is likely that most of these decisions are based on

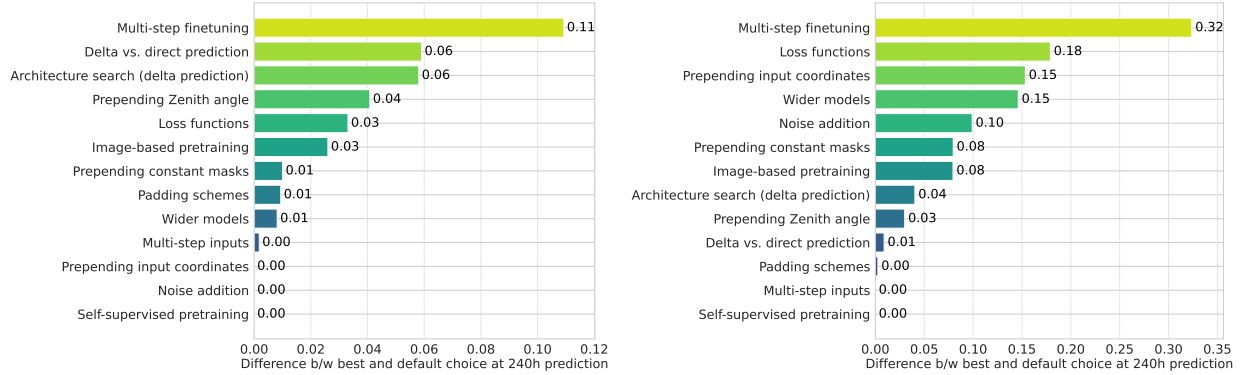


Figure 1: **Geometric ACC (left) and RMSE (right) for comparison between design choices.** This figure highlights the marginal contribution between the default choice (primarily based on our default 4-block UNet) and the best possible choice when considering different design decisions explored in this work. In cases where the default decision turned out to be the best, the marginal contribution is zero. Interestingly, there is a significant difference in the marginal contribution of different design choices between the two metrics.

experimental evidence that was not directly presented, comparing these choices on an even playing field is important to understand the marginal contribution of each of these design choices on the resulting model.

In this work, we take a step back and ask: *which of these choices are important and relevant for deep-learning-based weather forecasting systems?* To answer this question, we evaluate different aspects of the design space given a fixed number of training steps, including output formulation (direct, or residual prediction), model architecture, pretraining objective, image-based pretraining, loss functions, noise-based augmentations, zenith angle, constant masks, multi-step inputs, multi-step fine-tuning, as well as training on larger datasets. Our results predominantly indicate that highly-optimized computer-vision-based fixed-grid models are still effective for weather forecasting when evaluated on fixed grids, and the final performance of the models is more sensitive to some choices compared to others. These results call for extensive advancements in operator learning architecture design, for which we propose a new architecture through directly generalizing fixed-grid models (Liu-Schiaffini et al., 2024; Li et al., 2024b).

An overview of our results is presented in Fig. 1 where we compare the best choice in each category with the default choice (which is primarily based on our 4-block UNet architecture). Our results show that some of these choices have a non-trivial impact on the resulting model. Furthermore, we see that the two metrics i.e., geometric ACC and RMSE behave differently under different choices. In particular, our findings can be summarized as:

- For short-horizon prediction such as 6h considered in this work, training the model to predict the residual to the input state is much more efficient as compared to directly predicting the output for a range of different architectures (Section 4.1).
- Fixed-grid architectures including convolutional (such as UNet (Ronneberger et al., 2015), and ResNet-50 with fully convolutional decoder (Long et al., 2015)) and transformer-based models (such as Segformer (Zheng et al., 2021), and SETR (Zheng et al., 2021)) are more performant for weather forecasting on ERA5 dataset in contrast to grid-invariant models including graph-based (Lam et al., 2022), and operator-based (Pathak et al., 2022; Bonev et al., 2023) models when considering a fixed computational budget of 10 epochs, indicating a great need for

further architectural developments in grid-invariant models. We therefore present a hybrid architecture that combines the flexibility of grid-invariant architectures with the performance of grid-invariant models through a direct generalization of fixed-grid models (Liu-Schiaffini et al., 2024; Li et al., 2024b) (Section 4.2).

- Supervised training achieves superior performance compared to self-supervised pretraining using different objectives such as auto-encoding (Erhan et al., 2009), denoising auto-encoding (Erhan et al., 2009), or masked auto-encoding (He et al., 2022) (Section 4.3).
- Image-based pertaining can provide significant performance gains in some cases, specifically for transformers, as the model can still leverage its understanding of locality and attention while reinitializing the input and output heads to match the dimensionality of the ERA5 inputs as compared to RGB images (Section 4.4).
- Taking multiple previous input steps as input can increase the model’s propensity to overfit the task, and hence, degrade performance rather than improve it in many cases (Section 4.5).
- Zenith angle captures the location of the sun w.r.t. the query location, and hence, provides a notion of time for the model. Therefore, providing the zenith angle as an additional channel to the model provides significant gains at all prediction horizons (Section 4.6).
- Information about the geometry of the sphere can be encoded in the form of padding schemes used for image-based models. Using the circular pad for the longitude (x-axis) and zero/reflection padding scheme for the latitude (y-axis) for convolutional layers provides the best performance (Section 4.7).
- Injection of noise during training (which was primarily used for ensemble generation in prior work (Pathak et al., 2022; Bi et al., 2022)) can improve forecasting performance by increasing the model’s stability during long auto-regressive rollouts (Section 4.8).
- Providing information regarding the 3D coordinates on the sphere provides stability in the long-horizon auto-regressive rollouts potentially due to the model leveraging information regarding oversampling at the poles (Section 4.9).
- Variants of  $L_1$  loss function are more stable when doing longer auto-regressive rollouts as compared to MSE potentially due to them being less susceptible to outliers (Section 4.10).
- Inclusion of constant masks such as topography, soil type, and land-sea mask as commonly included in prior work (Bi et al., 2022) mostly degrades performance, potentially due to an increased propensity of the model to overfit (Section 4.11).
- Wider models outperform their narrower counterparts, similar to the findings in the computer vision literature (Zagoruyko & Komodakis, 2016) (Section 4.12).
- Multi-step fine-tuning on longer horizons helps in reducing model artifacts during long auto-regressive rollouts. This sequential fine-tuning outperforms models trained directly on a larger temporal resolution, as proposed in Bi et al. (2022). Furthermore, intermediate-step supervision is useful in some cases (particularly for our larger model) as compared to just last-step supervision (Section 4.13).
- Increasing the amount of data used for training improves performance. In some cases, this gain in performance is proportional to the gain in performance achieved by appropriately scaling

the number of training epochs on the smaller dataset to match the total training steps in the two cases (Section 4.15).

We believe that our findings would enable a better understanding of the design space of deep-learning-based weather forecasting systems and hence, the development of more efficient and effective systems in the future.

## 2 Related Work

Weyn et al. (2020) established some of the initial results on deep-learning-based weather forecasting. Their model was trained on  $2^\circ \times 2^\circ$ , and consumed two previous input states to produce a forecast for the next two states, each with a 6h stride. Their architecture was based on UNet, borrowing motivation from Larraondo et al. (2019) who compared three different encoder-decoder segmentation models to establish the utility of the UNet model for predicting precipitation fields given only geopotential height field on small input size of  $80 \times 120$  (focusing only on Europe). Rasp & Thuerey (2021) used a ResNet model on WeatherBench dataset (Rasp et al., 2020), achieving state-of-the-art performance for a data-driven method at a small resolution of  $5.625^\circ$  and a forecasting horizon of 5 days. These works showed that deep-learning-based models fall short of the performance of the operational IFS system.

FourCastNet (Pathak et al., 2022) was one of the first deep-learning-based weather forecasting systems to match the performance of the operational IFS system on spatially high-resolution inputs ( $0.25^\circ \times 0.25^\circ$ ) while being orders of magnitude faster at inference time. FourCastNet was based on (Adaptive) Fourier Neural Operator (Li et al., 2020a; Guibas et al., 2021) which is particularly designed to learn solution operators of differential equations, owing to its ability to be grid invariant. The model was trained for 6h prediction and fine-tuned for multi-step auto-regressive prediction. They trained the model using latitude-weighted MSE and summed up the losses from the two-step rollout during fine-tuning. They explored using additive Gaussian noise to the input state to generate an ensemble prediction (Graubner et al., 2022).

Pangu-weather (Bi et al., 2022) was based on the Swin transformer architecture (Liu et al., 2021), replacing the general position embedding with an earth-specific positional embedding. They trained 4 models with different prediction horizons including 6h, 12h, 18h, and 24h. The final prediction was based on a greedy combination of these fixed-stride models. The model was trained for 100 epochs on hourly sampled data. An ensemble of model predictions was constructed by adding Perlin (Perlin, 2002) noise to the input states.

Spherical Fourier Neural Operator (SFNO) (Bonev et al., 2023) proposed an extension of the Fourier neural operator based on spherical harmonics, taking into account the geometrical properties of Earth, which ultimately resulted in more stable prediction over longer horizons. Such a model is discretization agnostic, meaning it can be trained on various discretization of input functions, and the output functions can be queried at any discretization. The model was again pretrained for 6h prediction, and subsequently fine-tuned for multi-step auto-regressive predictions.

FuXi (Chen et al., 2023) focused on a 15-day forecasting task, and proposed a cascaded ML weather forecasting system that produced 15-day global forecasting on par with the ECMWF ensemble mean at a temporal resolution of 6h and spatial resolution of  $0.25^\circ \times 0.25^\circ$ . FuXi ensemble was created by perturbing both the initial states using Perlin noise (Perlin, 2002) as well as the model parameters using dropout (Srivastava et al., 2014). FuXi used the two previous time-steps to forecast the next step. Due to the 6h forecasting horizon, it required 60 auto-regressive steps for the model to generate a 15-day forecast. Focusing on previous work which argued that a single model is sub-optimal for both short-term and long-term horizons, they proposed a cascade model architecture

using pretrained FuXi models finetuned for optimal performance in specific 5-day forecast time windows: FuXi short (0-5 days), FuXi medium (5-10 days), and FuXi long (10-15 days). FuXi used cube embedding (similar to PanguWeather where they used cube patches) and a U-transformer (Petit et al., 2021). They trained the model for 40k steps on 8 GPUs.

Based on the success of graph-based message-passing networks (Gilmer et al., 2017), Lam et al. (2022) presented GraphCast model powered by a message-passing GNN, using a fixed multi-level mesh for efficient message-passing at multiple levels (Li et al., 2020c). GraphCast used 5 surface variables and 6 variables at 37 pressure levels, resulting in a total of 227 input channels. GraphCast took two previous time-steps as input and was trained for 300k steps with one auto-regressive step and subsequently fine-tuned for 1000 training steps with an increasing number of auto-regressive steps up to 12 steps (equivalent to a 3-day rollout).

More recently, GenCast (Price et al., 2023) trained GraphCast architecture (Lam et al., 2022) using the diffusion objective, providing probabilistic predictions instead of just deterministic outputs. The noise for the diffusion process is sampled from a sphere. Training a diffusion model produces detailed outputs with physically consistent power spectra, and avoids the over-smoothing of predictions returned by GraphCast (and all other deterministic forecasting systems) at longer prediction horizons. They trained this model on a lower resolution of  $1^\circ \times 1^\circ$  with a 12h prediction horizon using two previous steps as input. They used only 6 variables at 13 pressure levels instead of the 37 levels used in the original GraphCast model. One surprising thing to note is that this formulation allowed the model to work well even without multi-step fine-tuning. Similarly, Li et al. (2024a) used diffusion models as probabilistic forecasting systems, allowing natural generation of prediction ensembles using diffusion sampling in contrast to input state perturbation as done in prior work (Pathak et al., 2022; Bi et al., 2022).

NeuralGCM (Kochkov et al., 2023) attempted to learn General Circulation Models (GCMs), and proposed splitting the forecasting system into a dynamical core that simulates large-scale fluid motion and thermodynamics, and a learned physics model that predicts the effects of unresolved processes such as cloud formulation and precipitation, which are then fed to an ODE solver. This achieves performance comparable to other ML-based systems at shorter horizons (1-10 days), while still being effective at climate modeling spanning over multiple decades.

CoreDiff (Mardani et al., 2023) proposed a two-step regional forecasting system where a UNet first predicts the mean, which is subsequently corrected by a diffusion model. This formulation allows them to focus on km-scale atmospheric downscaling, while prior works focused on  $\sim 27.75$  km global weather prediction ( $0.25^\circ \times 0.25^\circ$ ). Many national weather agencies couple km-scale numerical weather models in a limited domain to coarser resolution models, known as ‘dynamical downscaling’.

DiffDA (Huang et al., 2024) is a method designed for data assimilation that assimilates atmospheric variables using predicted states and sparse observations. They used GraphCast as a pretrained model for diffusion. DiffDA was designed to produce assimilated global atmospheric data consistent with observations at  $0.25^\circ \times 0.25^\circ$  resolution globally. They used a conditional diffusion model where conditioning is on the current state, and the target is to predict the state after taking into account additional sparse observations. They considered 6 pressure-level variables and 4 surface variables, with a horizontal resolution of  $0.25^\circ$  and 13 vertical levels  $13 \times 6 + 4 = 82$  which matches the resolution of the WeatherBench-2 (Rasp et al., 2023) dataset. The model was trained for 20 epochs on 48 NVIDIA A100 GPUs using a batch size of 48.

Bodnar et al. (2024) proposed ‘Aurora’, which is a foundation model for atmospheric modeling, including weather forecasting, leveraging 3D Swin Transformer (Liu et al., 2021). The model is simultaneously trained on multiple datasets with different resolutions, variables, and pressure levels. The model is then fine-tuned using LoRA for downstream tasks. Aurora (Bodnar et al., 2024) outperforms GraphCast (Lam et al., 2022) on the vast majority of targets.

Vaughan et al. (2024) proposed an end-to-end weather forecasting system, ‘Aardvark’, to replace the entire operational NWP pipeline. Aardvark directly ingests raw observations and is capable of outputting global gridded forecasts, as well as local station forecasts.

In contrast to all prior work that attempts to propose the best predictive model for weather forecasting, our aim is to develop a thorough understanding of the different design decisions involved in designing these systems and their potential impact on weather forecasting performance.

## 3 Methods

### 3.1 Models

Our evaluation considers a range of different architectures. We use custom UNet implementation (Ronneberger et al., 2015), UNO (Ashiqur Rahman et al., 2022) implementation from NeuralOperator package<sup>1</sup>, official SFNO implementation from the Makani codebase<sup>2</sup>, FourCastNet (Pathak et al., 2022), and GraphCast (Lam et al., 2022) from Modulus package<sup>3</sup>, official pseudo-code translated to PyTorch (Paszke et al., 2019) for Pangu-weather (Bi et al., 2022), official code for Point Transformer v3 (Wu et al., 2023), Octformer (Wang, 2023), ISNet (Qin et al., 2022), and Efficient ViT L2 (Cai et al., 2022), and MMSeg (Contributors, 2020) implementation of SETR (Zheng et al., 2021), ResNet-50 with fully-convolutional decoder (Long et al., 2015), and Segformer (B5) (Xie et al., 2021). Note that some architectures operate on patches, hence producing a lower resolution output (one prediction per patch rather than per pixel). We add a very lightweight upsampling network in these cases to upsample the outputs to match the input resolution.

We emphasize that prior work based on neural operators learn the operator map between function spaces and are capable of training and testing on various resolutions, a capability unique to these models. In this work, we mainly focus on a fixed resolution and do not explore the operator learning aspect of weather forecast.

### 3.2 Dataset

We use  $0.25^\circ \times 0.25^\circ$  resolution ERA-5 reanalysis dataset (Hersbach et al., 2020) from 1980-2018 sub-sampled with a 6-hour stride following prior work with snapshots at 0000, 0600, 1200, and 1800 UTC (Pathak et al., 2022; Bi et al., 2022; Lam et al., 2022). We use data from 1980-2016 for model training, 2017 for validation, and 2018 for out-of-sample test set. All evaluations presented in the paper are based on the 2018 out-of-sample test set. We used 73 input variables including 8 surface variables, and 5 variables (q, t, u, v, z) sampled at 13 pressure levels, making the final input size for each timestamp to be:  $721 \times 1440 \times 73$ . We standardize each input channel based on the per-channel mean and standard deviation computed on the entire dataset.

### 3.3 Additional channels

Zenith angle is appended as an extra channel to the input when enabled. Therefore, during autoregressive rollouts, we append a new zenith angle for each timestamp. The input location is similarly appended as a separate input channel. We evaluate the use of three constant masks, including land mask, soil type, and topography following Bi et al. (2022). For multi-step inputs, multiple steps are concatenated in the channel dimension. Therefore, the number of input channels is multiplied

---

<sup>1</sup><https://neuraloperator.github.io/neuraloperator/dev/index.html>

<sup>2</sup><https://github.com/NVIDIA/modulus-makani>

<sup>3</sup><https://github.com/NVIDIA/modulus>

by the number of input steps. Input location and constant masks are only appended once when using multi-step inputs as they are static channels. These additional channels only affect the number of input channels, while leaving the number of output channels intact as these channels are not predicted by the model.

### 3.4 Multi-step fine-tuning

We backpropagate through multiple auto-regressive steps when fine-tuning. By default, we supervise only the last step in the auto-regressive rollout. We also evaluate intermediate-step supervision, where for each intermediate step, we calculate a (discounted) loss with a discount factor  $\gamma$  of 0.9 starting from 1.0 for the first step i.e., the weight for step  $i$  is computed as  $w_i = \gamma^{i-1}$  for  $i \geq 1$ . Furthermore, when using intermediate step supervision, we also experiment with the use of scheduled sampling (Bengio et al., 2015) i.e., the input steps are a convex combination of the previous model prediction as well as the actual target in the dataset with a linear schedule starting at 0.9 for the target, and annealing it to 0 for the last epoch i.e., the weight for the prediction at different epochs is 0.1, 0.2, 0.3, ..., 1.0 for the 10 epochs.

### 3.5 Optimization

All models were trained via synchronous updates for 10 epochs on 128 H100 GPUs using a batch size of 1 per GPU (effective batch size of 128). We used AdamW for optimization with an initial learning rate of 0.001, cosine learning rate decay, and weight decay of 0.0001. Note that we did not tune the hyperparameters for each of the different architectures separately.

### 3.6 Loss functions

We evaluated the use of different loss functions for training including  $L_2^2$  i.e., Mean-Squared Error (MSE),  $L_1$ , along with their linear composition, and their combinations such as Huber loss (Huber, 1992). For the ground truth next time-step weather state  $\mathbf{y}$  and the model forecast  $\hat{\mathbf{y}}$ ,  $L_2^2$  and  $L_1$  losses are defined as:

$$\mathcal{L}_2^2(\hat{\mathbf{y}}, \mathbf{y}) = \frac{1}{HWC} \sum_{h=1}^H \sum_{w=1}^W \sum_{c=1}^C (\hat{\mathbf{y}}_{h,w,c} - \mathbf{y}_{h,w,c})^2 \quad (1)$$

$$\mathcal{L}_1(\hat{\mathbf{y}}, \mathbf{y}) = \frac{1}{HWC} \sum_{h=1}^H \sum_{w=1}^W \sum_{c=1}^C |\hat{\mathbf{y}}_{h,w,c} - \mathbf{y}_{h,w,c}| \quad (2)$$

Huber loss is defined as:

$$\mathcal{L}_H(\hat{\mathbf{y}}, \mathbf{y}) = \frac{1}{HWC} \sum_{h=1}^H \sum_{w=1}^W \sum_{c=1}^C \begin{cases} \frac{1}{2}(\hat{\mathbf{y}}_{h,w,c} - \mathbf{y}_{h,w,c})^2 & \text{if } |\hat{\mathbf{y}}_{h,w,c} - \mathbf{y}_{h,w,c}| \leq \delta \\ \delta(|\hat{\mathbf{y}}_{h,w,c} - \mathbf{y}_{h,w,c}| - \frac{\delta}{2}) & \text{otherwise} \end{cases} \quad (3)$$

Following the function view of the problem, i.e., the variables are in fact functions defined everywhere on the sphere for which we only have access to their pointwise evaluation on a grid, we also explored training using geometric  $L_2^2$  and  $L_1$  losses. For a given quadrature rule  $w$ :

$$w(i) = \frac{\cos(\text{lat}(i))}{\frac{1}{H} \sum_{j=1}^H \cos(\text{lat}(j))} \quad (4)$$

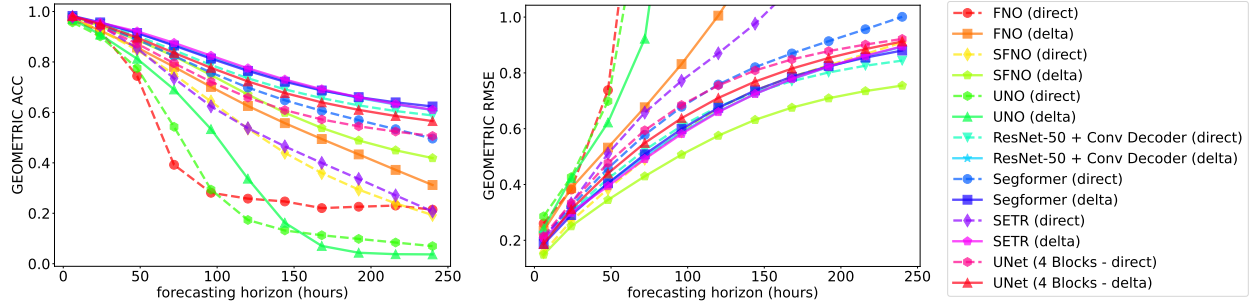


Figure 2: **Geometric ACC (left) and RMSE (right) for comparison between direct and delta prediction formulations.** The figure highlights that delta prediction is almost always superior in terms of performance as compared to direct prediction at the 6h prediction horizon (results in tabular form are presented in Table 2).

$$\mathcal{L}(\hat{\mathbf{y}}, \mathbf{y}) = \frac{1}{HW C} \sum_{h=1}^H w(h) \sum_{w=1}^W \sum_{c=1}^C \mathcal{L}'(\hat{\mathbf{y}}_{h,w,c}, \mathbf{y}_{h,w,c}) \quad (5)$$

where inner  $\mathcal{L}'$  is either  $\frac{1}{2}(\cdot)^2$  for the  $L_2^2$  loss on function spaces, and  $|\cdot|$  for  $L_1$  on function spaces. These quadrature rules have been frequently used in the past (Pathak et al., 2022; Bi et al., 2022; Lam et al., 2022; Nguyen et al., 2023b).

### 3.7 Metrics

We report geometric (latitude-weighted) Anomaly Correlation Coefficient (ACC), and Root Mean-Squared Error (RMSE), where the latitudes are weighted according to the latitude value (Rasp et al., 2020; Nguyen et al., 2023b) (see Eq. 5). ACC is defined as:

$$\text{ACC}(\hat{\mathbf{y}}, \mathbf{y}) = \frac{1}{C} \sum_{c=1}^C \frac{\frac{1}{HW} \sum_{h=1}^H w(h) \sum_{w=1}^W (\hat{\mathbf{y}}_{h,w,c} \times \mathbf{y}_{h,w,c})}{\sqrt{\frac{1}{HW} \sum_{h=1}^H w(h) \sum_{w=1}^W \hat{\mathbf{y}}_{h,w,c}^2} \sqrt{\frac{1}{HW} \sum_{h=1}^H w(h) \sum_{w=1}^W \mathbf{y}_{h,w,c}^2}} \quad (6)$$

These two metrics allow for assessing the quality of the trained model. In particular, ACC considers the climatology-corrected correlation between the ground truth and model forecast, and RMSE considers the quantitative differences between the two fields. Since each channel is normalized, we report the mean RMSE and ACC across all 73 input channels.

## 4 Experiments

Our evaluation focuses on analyzing different aspects of the design space, starting from evaluating the impact of different problem formulations (Section 4.1), model architecture (Section 4.2), self-supervised pretraining objectives (Section 4.3), image-based pretraining (Section 4.4), multi-step inputs (Section 4.5), zenith angle as an additional input channel (Section 4.6), padding schemes for the convolutional layers (Section 4.7), noise addition to the input states (Section 4.8), auxiliary information regarding the 3D coordinates on the sphere (Section 4.9), loss functions (Section 4.10), additional auxiliary static channels such as soil type, land-sea mask, and topography (Section 4.11), wider models by increasing the hidden dimension (Section 4.12), multi-step fine-tuning including models operating at a larger prediction horizon (Section 4.13), comparison of different models with multi-step fine-tuning (Section 4.14), and training on a larger hourly dataset (Section 4.15).

Model Name	# of Parameters
FNO (Li et al., 2020a)	233,039,081
FourCastNet (Pathak et al., 2022)	79,900,416
SFNO (Bonev et al., 2023)	289,392,337
UNO (Ashiqur Rahman et al., 2022)	145,418,729
ISNet (Qin et al., 2022)	45,114,917
ResNet-50 + Fully Convolutional Decoder (Long et al., 2015)	47,202,505
Segformer (Xie et al., 2021)	82,208,137
Segmentation Transformer (SETR) (Zheng et al., 2021)	343,751,497
Swin Transformer (Liu et al., 2021)	59,086,083
Efficient ViT L2 (Cai et al., 2022)	51,403,689
PanguWeather (Bi et al., 2022)	64,247,821
UNet (4 Layers) (Ronneberger et al., 2015)	47,152,969
UNet (5 Blocks) (Ronneberger et al., 2015)	399,563,977
UNet (4 Layers - 128-dim initial projection) (Ronneberger et al., 2015)	188,520,649
UNet (5 Blocks - 128-dim initial projection) (Ronneberger et al., 2015)	1,598,034,889
GraphCast (Lam et al., 2022)	8,866,377
Point Transformer v3 (Wu et al., 2023)	46,439,017
Octformer (Wang, 2023)	40,497,325
Graph UNet (4 Blocks) (Ronneberger et al., 2015)	47,377,417
Graph UNet (5 Blocks) (Ronneberger et al., 2015)	399,788,425

Table 1: **Total number of parameters in different models evaluated in our work.** Note that the number of parameters is not directly proportional to the memory footprint.

We always train the model using Mean-Squared Error (MSE) loss unless specified otherwise. The number of parameters in the different models tested is presented in Table 1 for reference. Note that the number of parameters is not directly proportional to the memory footprint for that model. A notable example is GraphCast (Lam et al., 2022), which has only a small number of parameters, but a very significant memory footprint.

As these sections are relatively independent, one can look at the sections independently without going through the others.

#### 4.1 Impact of formulation

Direct prediction refers to the case where we directly generate the next weather state conditioned on the previous state(s). More concretely,  $\mathbf{s}_t = \Phi(\mathbf{s}_{t-1})$  where  $\Phi$  represents the deep-learning-based weather forecasting system. This has been a common choice for prior high-resolution models (Pathak et al., 2022; Bonev et al., 2023; Bi et al., 2022; Lam et al., 2022).

Delta prediction refers to the case where we predict the change to be made to the previous state considering the weather forecasting to be discretization of a continuous-time process (Chen et al., 2018). More concretely,  $\mathbf{s}_t = \mathbf{s}_{t-1} + \Phi(\mathbf{s}_{t-1})$  where  $\Phi$  represents the deep-learning-based weather forecasting system. Note that this residual prediction is distinct from residual layers used within the model architecture. Residual prediction for weather forecasting has also been explored in the recent past (Nguyen et al., 2023b). However, we attempt to disentangle the precise impact of residual prediction instead of directly using it as our proposed approach.

The geometric ACC and RMSE for direct vs. delta prediction on selected architectures are

Model	Forecasting horizon (hours)										
	6	24	48	72	96	120	144	168	192	216	240
FNO (direct)	0.9650	0.9231	0.7446	0.3922	0.2812	0.2580	0.2469	0.2205	0.2260	0.2306	0.2142
FNO (delta)	0.9722	0.9244	0.8571	0.7805	0.7010	0.6255	0.5573	0.4944	0.4334	0.3721	0.3121
SFNO (direct)	0.9743	0.9255	0.8478	0.7512	0.6432	0.5358	0.4396	0.3593	0.2939	0.2395	0.1930
SFNO (delta)	0.9801	0.9422	0.8879	0.8227	0.7482	0.6709	0.5988	0.5383	0.4888	0.4497	0.4189
UNO (direct)	0.9571	0.9012	0.7755	0.5427	0.2938	0.1734	0.1319	0.1128	0.0984	0.0841	0.0697
UNO (delta)	0.9701	0.9083	0.8126	0.6909	0.5337	0.3371	0.1625	0.0705	0.0435	0.0378	0.0370
ResNet-50 + Conv Decoder (direct)	0.9757	0.9506	0.9034	0.8465	0.7881	0.7353	0.6913	0.6565	0.6278	0.6053	0.5880
ResNet-50 + Conv Decoder (delta)	0.9801	0.9539	0.9150	0.8679	0.8177	0.7692	0.7257	0.6884	0.6572	0.6313	0.6094
Segformer (direct)	0.9780	0.9454	0.8894	0.8241	0.7582	0.6984	0.6481	0.6064	0.5691	0.5334	0.4961
Segformer (delta)	<b>0.9825</b>	<b>0.9568</b>	0.9149	0.8650	0.8132	0.7645	0.7215	0.6869	<b>0.6604</b>	<b>0.6398</b>	<b>0.6236</b>
SETR (direct)	0.9789	0.9448	0.8543	0.7349	0.6240	0.5375	0.4653	0.3996	0.3361	0.2710	0.2071
SETR (delta)	0.9789	0.9559	<b>0.9211</b>	<b>0.8756</b>	<b>0.8248</b>	<b>0.7748</b>	<b>0.7302</b>	<b>0.6917</b>	0.6598	0.6327	0.6102
UNet (4 Blocks - direct)	0.9760	0.9408	0.8725	0.7948	0.7215	0.6588	0.6090	0.5720	0.5449	0.5239	0.5064
UNet (4 Blocks - delta)	0.9820	0.9495	0.8965	0.8360	0.7768	0.7228	0.6767	0.6398	0.6100	0.5858	0.5655

(a) Geometric ACC

Model	Forecasting horizon (hours)										
	6	24	48	72	96	120	144	168	192	216	240
FNO (direct)	0.2602	0.3820	0.7381	1.7854	3.4580	5.7151	8.1361	12.5979	19.2537	26.5092	38.7152
FNO (delta)	0.2346	0.3867	0.5322	0.6768	0.8314	1.0052	1.2096	1.4664	1.8029	2.2588	2.8828
SFNO (direct)	0.1575	0.2694	0.3844	0.4922	0.5900	0.6728	0.7373	0.7862	0.8273	0.8675	0.9094
SFNO (delta)	<b>0.1488</b>	<b>0.2506</b>	<b>0.3448</b>	<b>0.4295</b>	<b>0.5070</b>	<b>0.5751</b>	<b>0.6318</b>	<b>0.6755</b>	<b>0.7091</b>	<b>0.7348</b>	<b>0.7546</b>
UNO (direct)	0.2860	0.4266	0.6987	1.4600	2.9173	4.8864	7.6792	12.3996	21.8269	43.2852	96.2574
UNO (delta)	0.2429	0.4231	0.6223	0.9225	1.8544	7.8484	65.0581	663.3524	7056.8694	71029.8833	683521.7333
ResNet-50 + Conv Decoder (direct)	0.2162	0.3058	0.4203	0.5234	0.6101	0.6789	0.7311	0.7703	0.8016	0.8257	0.8441
ResNet-50 + Conv Decoder (delta)	0.1992	0.3012	0.4041	0.5006	0.5871	0.6618	0.7248	0.7774	0.8214	0.8594	0.8938
Segformer (direct)	0.2077	0.3219	0.4579	0.5780	0.6784	0.7584	0.8204	0.8698	0.9137	0.9564	1.0010
Segformer (delta)	0.1863	0.2902	0.4044	0.5082	0.5988	0.6748	0.7372	0.7861	0.8240	0.8548	0.8802
SETR (direct)	0.2061	0.3324	0.5108	0.6576	0.7716	0.8703	0.9763	1.1057	1.2576	1.4070	1.5149
SETR (delta)	0.2079	0.2989	0.3945	0.4916	0.5815	0.6598	0.7247	0.7784	0.8228	0.8615	0.8951
UNet (4 Blocks - direct)	0.2151	0.3333	0.4771	0.5942	0.6848	0.7550	0.8087	0.8484	0.8781	0.9015	0.9217
UNet (4 Blocks - delta)	0.1871	0.3113	0.4397	0.5488	0.6376	0.7103	0.7689	0.8154	0.8535	0.8853	0.9127

(b) Geometric RMSE

Table 2: **Geometric ACC (a) and RMSE (b) for comparison between direct and delta prediction formulations.** The table highlights that delta prediction is almost always superior in terms of performance as compared to direct prediction at the 6h prediction horizon (results in graphical form are presented in Fig. 2).

presented in Table 2 (Fig. 2). We see a clear trend in this case, with significantly better performance when using delta prediction compared to direct prediction. Fixed-grid models including UNet (Ronneberger et al., 2015), ResNet-50 with fully-convolutional decoder (Long et al., 2015), SEgmentation TRansformer (SETR) (Zheng et al., 2021), and Segformer (Xie et al., 2021) perform better than other alternate architectures with only minor differences in performance between them. One notable exception is the Spherical Fourier Neural Operator (SFNO) (Bonev et al., 2023) which achieves the lowest geometric RMSE, potentially due to correct modeling at the poles as it integrates geometric properties of the sphere<sup>4</sup>.

Using delta prediction essentially diminishes the performance difference between residual and non-residual architectures. These results establish the utility of delta prediction compared to direct prediction (even for residual architectures) given the slow evolution of weather states at small prediction horizons (we used a prediction horizon of just 6 hours to train these models). We expect diminishing improvements with delta prediction for larger prediction horizons due to significant changes in the weather state, which we consider to be an interesting direction to investigate further

<sup>4</sup>Note that we use the official SFNO repository to report SFNO results, therefore, while we attempted to minimize differences, the significantly lower RMSE might have been the result of differences in implementation. For this reason, we avoid making any claims about this result, and exclude it from discussion.

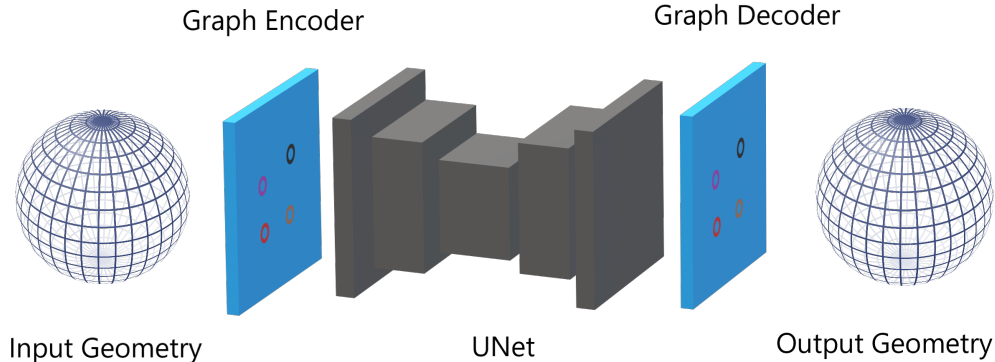


Figure 3: **Graph UNet architecture** where a fixed-grid UNet architecture is sandwiched between grid-invariant graph encoder and decoder layers. This provides the model with the flexibility of being grid-invariant while retaining the performance of fixed-grid models.

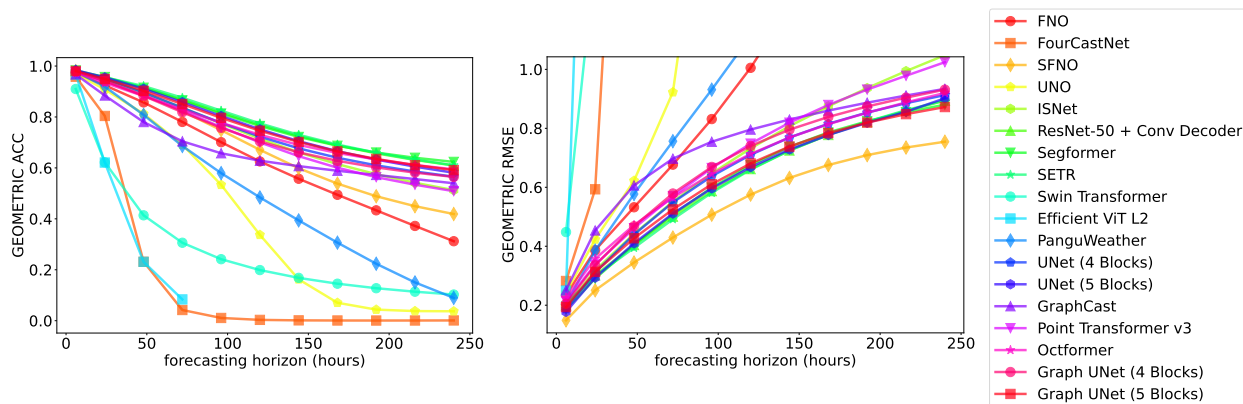


Figure 4: **Geometric ACC (left) and RMSE (right) for comparison of different architectures when using the delta prediction formulation.** The figure highlights that some architectures such as Segformer, SETR, ResNet-50 w/ convolutional decoder, and UNet are more efficient and effective for weather forecasting given a small and fixed number of training steps that we focused on in this work (results in tabular form are presented in Table 3).

in the future.

Given the utility of delta prediction in our case, all subsequent experiments use delta prediction as the formulation unless mentioned otherwise. We will explore more architectures for this task in the next sub-section.

## 4.2 Evaluation of different model architectures

Prior work on high-resolution weather forecasting explored different architecture, ranging from Adaptive Fourier Neural Operators (Pathak et al., 2022), Spherical Fourier Neural Operators (Bonev et al., 2023), Vision Transformer (Bi et al., 2022; Nguyen et al., 2023a), and message-passing GNNs (Lam et al., 2022; Price et al., 2023). Note that the large input size used for high-resolution weather forecasting makes some architectures more applicable to this problem due to memory constraints. Therefore, we further expand on the list of architectures explored in the last section. Given the established utility of delta prediction, we only focus on delta prediction in this case.

In particular, we consider three different model families. The first type of models considered

Model	Forecasting horizon (hours)										
	6	24	48	72	96	120	144	168	192	216	240
FNO	0.9722	0.9244	0.8571	0.7805	0.7010	0.6255	0.5573	0.4944	0.4334	0.3721	0.3121
FourCastNet	0.9581	0.8040	0.2314	0.0420	0.0107	0.0032	0.0013	0.0008	0.0006	0.0008	0.0010
SFNO	0.9801	0.9422	0.8879	0.8227	0.7482	0.6709	0.5988	0.5383	0.4888	0.4497	0.4189
UNO	0.9701	0.9083	0.8126	0.6909	0.5337	0.3371	0.1625	0.0705	0.0435	0.0378	0.0370
ISNet	0.9806	0.9471	0.8957	0.8362	0.7745	0.7147	0.6610	0.6149	0.5753	0.5416	0.5127
ResNet-50 + Conv Decoder	0.9801	0.9539	0.9150	0.8679	0.8177	0.7692	0.7257	0.6884	0.6572	0.6313	0.6094
Segformer	0.9825	<b>0.9568</b>	0.9149	0.8650	0.8132	0.7645	0.7215	0.6869	0.6604	0.6398	0.6236
SETR	0.9789	0.9559	<b>0.9211</b>	<b>0.8756</b>	0.8248	0.7748	0.7302	0.6917	0.6598	0.6327	0.6102
Swin Transformer	0.9099	0.6219	0.4138	0.3061	0.2415	0.1988	0.1682	0.1453	0.1276	0.1139	0.1028
Efficient ViT L2	0.9669	0.6210	0.2311	0.0836	nan						
PanguWeather	0.9785	0.9191	0.8082	0.6861	0.5794	0.4841	0.3939	0.3065	0.2237	0.1503	0.0897
UNet (4 Blocks)	0.9820	0.9495	0.8965	0.8360	0.7768	0.7228	0.6767	0.6398	0.6100	0.5858	0.5655
UNet (5 Blocks)	<b>0.9838</b>	0.9554	0.9105	0.8581	0.8038	0.7517	0.7050	0.6656	0.6327	0.6049	0.5809
GraphCast	0.9672	0.8843	0.7801	0.7044	0.6575	0.6282	0.6070	0.5888	0.5723	0.5561	0.5397
Point Transformer v3	0.9764	0.9404	0.8861	0.8243	0.7606	0.7000	0.6460	0.6007	0.5637	0.5340	0.5086
Octformer	0.9737	0.9340	0.8823	0.8294	0.7773	0.7299	0.6903	0.6586	0.6331	0.6115	0.5943
Graph UNet (4 Blocks)	0.9781	0.9412	0.8827	0.8185	0.7571	0.7040	0.6611	0.6278	0.6020	0.5814	0.5646
Graph UNet (5 Blocks)	0.9807	0.9492	0.9029	0.8508	0.7966	0.7461	0.7018	0.6649	0.6353	0.6110	0.5913

(a) Geometric ACC

Model	Forecasting horizon (hours)										
	6	24	48	72	96	120	144	168	192	216	240
FNO	0.2346	0.3867	0.5322	0.6768	0.8314	1.0052	1.2096	1.4664	1.8029	2.2588	2.8828
FourCastNet	0.2822	0.5932	2.8587	15.3645	54.4597	172.6959	531.8129	1542.8602	4298.7569	11823.4250	32522.8528
SFNO	<b>0.1488</b>	<b>0.2506</b>	<b>0.3448</b>	<b>0.4295</b>	<b>0.5070</b>	<b>0.5751</b>	<b>0.6318</b>	<b>0.6755</b>	<b>0.7091</b>	<b>0.7348</b>	<b>0.7546</b>
UNO	0.2429	0.4231	0.6223	0.9225	1.8544	7.8484	65.0581	663.3524	7056.8694	71029.8833	683521.7333
ISNet	0.1952	0.3186	0.4421	0.5511	0.6469	0.7319	0.8072	0.8745	0.9365	0.9941	1.0481
ResNet-50 + Conv Decoder	0.1992	0.3012	0.4041	0.5006	0.5871	0.6618	0.7248	0.7774	0.8214	0.8594	0.8938
Segformer	0.1863	0.2902	0.4044	0.5082	0.5988	0.6748	0.7372	0.7861	0.8240	0.8548	0.8802
SETR	0.2079	0.2989	0.3945	0.4916	0.5815	0.6598	0.7247	0.7784	0.8228	0.8615	0.8951
Swin Transformer	0.4481	1.3812	2.5692	3.7529	4.9411	6.1339	7.3301	8.5284	9.7282	10.9290	12.1305
Efficient ViT L2	0.2496	3.1187	4112.0438	9155085.9130	nan						
PanguWeather	0.2036	0.3854	0.5772	0.7563	0.9313	1.1134	1.3104	1.5293	1.8021	2.2216	3.0362
UNet (4 Blocks)	0.1871	0.3113	0.4397	0.5488	0.6376	0.7103	0.7689	0.8154	0.8535	0.8853	0.9127
UNet (5 Blocks)	0.1774	0.2933	0.4099	0.5109	0.5964	0.6683	0.7281	0.7773	0.8188	0.8561	0.9019
GraphCast	0.2507	0.4536	0.6064	0.6971	0.7545	0.7958	0.8298	0.8601	0.8870	0.9113	0.9338
Point Transformer v3	0.2141	0.3378	0.4610	0.5696	0.6653	0.7481	0.8190	0.8792	0.9314	0.9783	1.0243
Octformer	0.2262	0.3574	0.4720	0.5652	0.6453	0.7131	0.7689	0.8140	0.8528	0.8880	0.9200
Graph UNet (4 Blocks)	0.2051	0.3353	0.4679	0.5789	0.6690	0.7401	0.7955	0.8386	0.8742	0.9042	0.9312
Graph UNet (5 Blocks)	0.1937	0.3129	0.4271	0.5250	0.6103	0.6809	0.7381	0.7836	0.8195	0.8481	0.8722

(b) Geometric RSME

Table 3: **Geometric ACC (a) and RMSE (b) for comparison of different architectures when using the delta prediction formulation.** The table highlights that some architectures such as Segformer, SETR, ResNet-50 w/ convolutional decoder, and UNet are more efficient and effective for weather forecasting given a small and fixed number of training steps that we focused on in this work (results in graphical form are presented in Fig. 4).

are regular image-to-image models prevalent in the computer-vision literature, including variants of convolutional networks (LeCun et al., 1989; Ronneberger et al., 2015) such as UNet (Ronneberger et al., 2015) and ResNet-50 with convolutional decoder (Long et al., 2015), and variants of transformer architecture (Vaswani et al., 2017; Dosovitskiy et al., 2020) such as SEgementation TRansformer (SETR) (Zheng et al., 2021), Swin transformer (Liu et al., 2021), and Segformer (Xie et al., 2021).

The second type that we consider are architectures that directly operate on point clouds, such as graph neural networks (Gilmer et al., 2017), or point-transformers (Wu et al., 2023). In particular, we evaluate many variants of these architectures including point transformer v3 (Wu et al., 2023), Octformer (Wang, 2023), and message-passing GNNs (Gilmer et al., 2017) in the form

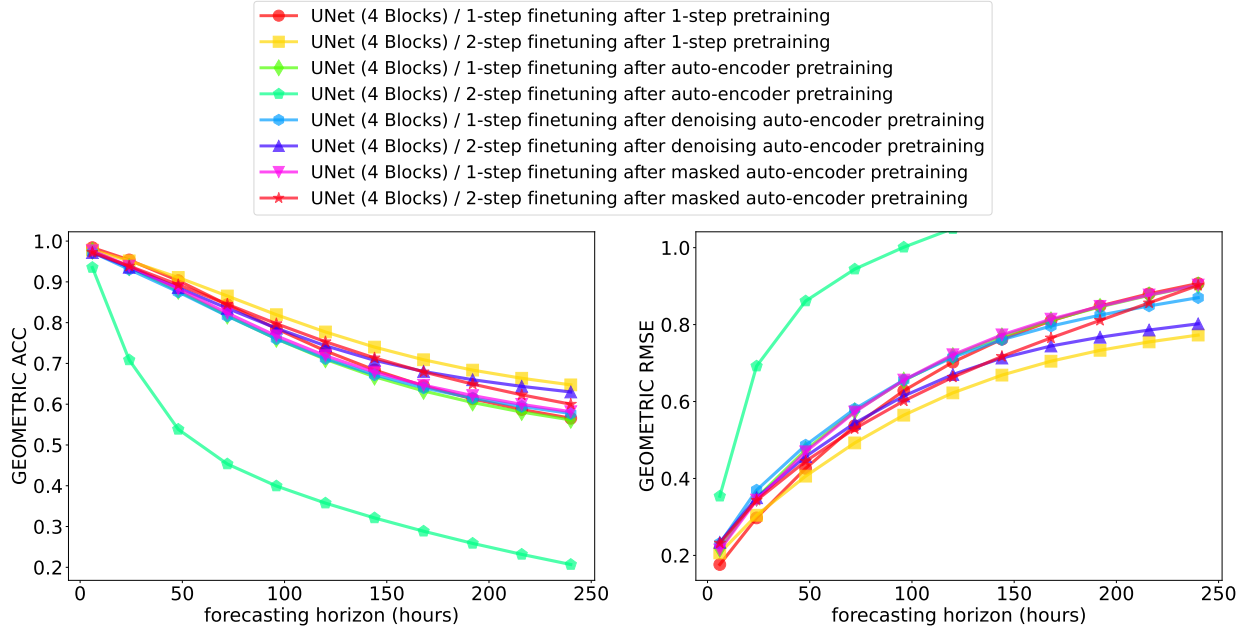


Figure 5: **Geometric ACC (left) and RMSE (right) for comparison of different pretraining objectives on UNet with 4 blocks.** The figure highlights that supervised pretraining achieves better performance in comparison to self-supervised pretraining using different objectives evaluated in our case (results in tabular form are presented in Table 4).

of GraphCast (Lam et al., 2022). To fit the GraphCast model fully within a single GPU, we used 256 hidden dimensions (the original implementation used 512 as the hidden dimension) and mixed precision for training in contrast to all other models that were trained in full precision i.e., FP32.

The third type focuses on operator-based models, primarily designed to learn solution operators of differential equations that are resolution invariant by construction (Li et al., 2020a; Ashiqur Rahman et al., 2022). FourCastNet (Pathak et al., 2022) is based on the (Adaptive) Fourier Neural Operator (FNO) (Li et al., 2020a; Guibas et al., 2021) model. We further test two other operator models including Spherical Fourier Neural Operator (SFNO) (Bonev et al., 2023), and U-shaped Neural Operator (UNO) (Ashiqur Rahman et al., 2022).

The geometric ACC and RMSE for residual prediction using a range of different architectures are presented in Table 3 (Fig. 4). The results primarily highlight that fixed-grid models are superior in terms of performance as compared to graph-based models. In particular, we see the dominant performance of UNet (Ronneberger et al., 2015), Segformer (Xie et al., 2021), SETR (Zheng et al., 2021), and ResNet-50 with a fully convolutional decoder (Long et al., 2015) at different stages. Note that these results are based on just single-step training for 10 epochs. Although one would prefer to train every model till convergence (or for a large number of epochs as commonly done in prior work (Pathak et al., 2022; Bi et al., 2022)), this is computationally infeasible. Therefore, our exploration which is compute-bound implicitly prioritizes more efficient learning architectures.

Due to the simplicity and prevalence of the UNet architecture, our future exploration focuses on UNet with residual prediction. As UNet loses the ability to be grid-invariant (Liu-Schiaffini et al., 2024), we also explore the coupling of UNet with a 2-layered graph neural operator layers as graph encoder and decoder (using  $k = 4$  for graph integration) (Li et al., 2020b) with the UNet model sandwiched in between, which we call ‘Graph UNet’ (see Fig. 3 for a visual illustration). Graph UNet retains the properties of being grid invariant via the graph encoder and decoder layers, while

Model	Forecasting horizon (hours)										
	6	24	48	72	96	120	144	168	192	216	240
UNet (4 Blocks) / 1-step finetuning after 1-step pretraining	<b>0.9839</b>	<b>0.9538</b>	0.9032	0.8440	0.7850	0.7308	0.6839	0.6449	0.6131	0.5869	0.5655
UNet (4 Blocks) / 2-step finetuning after 1-step pretraining	0.9779	0.9515	<b>0.9108</b>	<b>0.8654</b>	<b>0.8195</b>	<b>0.7771</b>	<b>0.7400</b>	<b>0.7090</b>	<b>0.6835</b>	<b>0.6636</b>	<b>0.6474</b>
UNet (4 Blocks) / 1-step finetuning after auto-encoder pretraining	0.9758	0.9359	0.8779	0.8171	0.7602	0.7100	0.6674	0.6325	0.6041	0.5808	0.5615
UNet (4 Blocks) / 2-step finetuning after auto-encoder pretraining	0.9352	0.7085	0.5383	0.4534	0.3993	0.3574	0.3211	0.2885	0.2587	0.2317	0.2069
UNet (4 Blocks) / 1-step finetuning after denoising auto-encoder pretraining	0.9723	0.9305	0.8753	0.8161	0.7605	0.7119	0.6720	0.6401	0.6149	0.5945	0.5772
UNet (4 Blocks) / 2-step finetuning after denoising auto-encoder pretraining	0.9718	0.9357	0.8862	0.8350	0.7863	0.7433	0.7077	0.6803	0.6600	0.6437	0.6300
UNet (4 Blocks) / 1-step finetuning after masked auto-encoder pretraining	0.9764	0.9386	0.8829	0.8236	0.7675	0.7189	0.6787	0.6465	0.6211	0.5995	0.5815
UNet (4 Blocks) / 2-step finetuning after masked auto-encoder pretraining	0.9723	0.9387	0.8931	0.8450	0.7974	0.7531	0.7135	0.6792	0.6493	0.6230	0.6000

(a) Geometric ACC

Model	Forecasting horizon (hours)										
	6	24	48	72	96	120	144	168	192	216	240
UNet (4 Blocks) / 1-step finetuning after 1-step pretraining	<b>0.1763</b>	<b>0.2975</b>	0.4262	0.5371	0.6281	0.7023	0.7620	0.8098	0.8483	0.8802	0.9068
UNet (4 Blocks) / 2-step finetuning after 1-step pretraining	0.2064	0.3044	<b>0.4060</b>	<b>0.4924</b>	<b>0.5646</b>	<b>0.6225</b>	<b>0.6687</b>	<b>0.7048</b>	<b>0.7332</b>	<b>0.7550</b>	<b>0.7728</b>
UNet (4 Blocks) / 1-step finetuning after auto-encoder pretraining	0.2169	0.3497	0.4743	0.5747	0.6545	0.7183	0.7696	0.8111	0.8460	0.8761	0.9021
UNet (4 Blocks) / 2-step finetuning after auto-encoder pretraining	0.3539	0.6921	0.8613	0.9442	1.0011	1.0495	1.0951	1.1395	1.1835	1.2271	1.2704
UNet (4 Blocks) / 1-step finetuning after denoising auto-encoder pretraining	0.2310	0.3696	0.4865	0.5808	0.6559	0.7151	0.7608	0.7961	0.8246	0.8485	0.8700
UNet (4 Blocks) / 2-step finetuning after denoising auto-encoder pretraining	0.2338	0.3499	0.4571	0.5439	0.6144	0.6702	0.7130	0.7443	0.7672	0.7858	0.8020
UNet (4 Blocks) / 1-step finetuning after masked auto-encoder pretraining	0.2141	0.3438	0.4693	0.5726	0.6557	0.7215	0.7732	0.8141	0.8474	0.8769	0.9027
UNet (4 Blocks) / 2-step finetuning after masked auto-encoder pretraining	0.2321	0.3432	0.4449	0.5295	0.6015	0.6633	0.7172	0.7653	0.8109	0.8564	0.9018

(b) Geometric RMSE

Table 4: **Geometric ACC (a) and RMSE (b) for comparison of different pretraining objectives on UNet with 4 blocks.** The table highlights that supervised pretraining achieves better performance in comparison to self-supervised pretraining using different objectives evaluated in our case (results in graphical form are presented in Fig. 5).

Model	Forecasting horizon (hours)										
	6	24	48	72	96	120	144	168	192	216	240
UNet (5 Blocks) / 1-step finetuning after 1-step pretraining	<b>0.9855</b>	0.9593	0.9180	0.8696	0.8192	0.7696	0.7252	0.6869	0.6557	0.6305	0.6099
UNet (5 Blocks) / 2-step finetuning after 1-step pretraining	0.9827	<b>0.9625</b>	<b>0.9286</b>	<b>0.8879</b>	<b>0.8453</b>	<b>0.8048</b>	<b>0.7685</b>	<b>0.7370</b>	<b>0.7104</b>	<b>0.6890</b>	<b>0.6717</b>
UNet (5 Blocks) / 1-step finetuning after auto-encoder pretraining	0.9787	0.9440	0.8919	0.8328	0.7742	0.7211	0.6764	0.6410	0.6139	0.5929	0.5754
UNet (5 Blocks) / 2-step finetuning after auto-encoder pretraining	0.9745	0.9459	0.9075	0.8640	0.8186	0.7756	0.7380	0.7057	0.6794	0.6584	0.6413
UNet (5 Blocks) / 1-step finetuning after denoising auto-encoder pretraining	0.9798	0.9469	0.8971	0.8392	0.7809	0.7270	0.6807	0.6421	0.6109	0.5855	0.5637
UNet (5 Blocks) / 2-step finetuning after denoising auto-encoder pretraining	0.9724	0.9389	0.8927	0.8430	0.7929	0.7462	0.7050	0.6703	0.6414	0.6174	0.5969
UNet (5 Blocks) / 1-step finetuning after masked auto-encoder pretraining	0.9793	0.9458	0.8947	0.8367	0.7792	0.7266	0.6815	0.6447	0.6148	0.5904	0.5692
UNet (5 Blocks) / 2-step finetuning after masked auto-encoder pretraining	0.9750	0.9467	0.9082	0.8649	0.8199	0.7770	0.7382	0.7049	0.6768	0.6539	0.6348

(a) Geometric ACC

Model	Forecasting horizon (hours)										
	6	24	48	72	96	120	144	168	192	216	240
UNet (5 Blocks) / 1-step finetuning after 1-step pretraining	<b>0.1681</b>	0.2806	0.3946	0.4929	0.5759	0.6466	0.7043	0.7516	0.7897	0.8209	0.8472
UNet (5 Blocks) / 2-step finetuning after 1-step pretraining	0.1825	<b>0.2693</b>	<b>0.3644</b>	<b>0.4480</b>	<b>0.5181</b>	<b>0.5752</b>	<b>0.6212</b>	<b>0.6582</b>	<b>0.6880</b>	<b>0.7113</b>	<b>0.7299</b>
UNet (5 Blocks) / 1-step finetuning after auto-encoder pretraining	0.2036	0.3272	0.4476	0.5513	0.6373	0.7074	0.7635	0.8076	0.8428	0.8717	0.8970
UNet (5 Blocks) / 2-step finetuning after auto-encoder pretraining	0.2229	0.3226	0.4138	0.4942	0.5641	0.6218	0.6676	0.7044	0.7330	0.7549	0.7725
UNet (5 Blocks) / 1-step finetuning after denoising auto-encoder pretraining	0.1984	0.3189	0.4401	0.5486	0.6414	0.7201	0.7866	0.8436	0.8935	0.9393	0.9834
UNet (5 Blocks) / 2-step finetuning after denoising auto-encoder pretraining	0.2317	0.3421	0.4449	0.5310	0.6038	0.6646	0.7147	0.7557	0.7896	0.8186	0.8449
UNet (5 Blocks) / 1-step finetuning after masked auto-encoder pretraining	0.2014	0.3228	0.4435	0.5466	0.6311	0.6998	0.7547	0.7983	0.8338	0.8638	0.8910
UNet (5 Blocks) / 2-step finetuning after masked auto-encoder pretraining	0.2208	0.3204	0.4135	0.4953	0.5664	0.6263	0.6760	0.7163	0.7493	0.7758	0.7981

(b) Geometric RMSE

Table 5: **Geometric ACC (a) and RMSE (b) for comparison of different pretraining objectives on UNet with 5 blocks.** The table highlights that supervised pretraining achieves better performance in comparison to self-supervised pretraining using different objectives evaluated in this work (results in graphical form are presented in Fig. 6).

still retaining the performance of the UNet model as seen by the model’s performance. Therefore, following the graph kernel operator learning (Li et al., 2020b) and adaptation of convolution neural networks to neural operators (Liu-Schiaffini et al., 2024), our model qualities as a neural operator. This result shows that hybrid architectures that combine the flexibility of grid-invariant models with the performance of fixed-grid models can be a lucrative direction for designing future weather forecasting systems. Based on these findings, we focus on the fixed-resolution models in this work, and train models without the graph encoder and decoder unless mentioned otherwise.

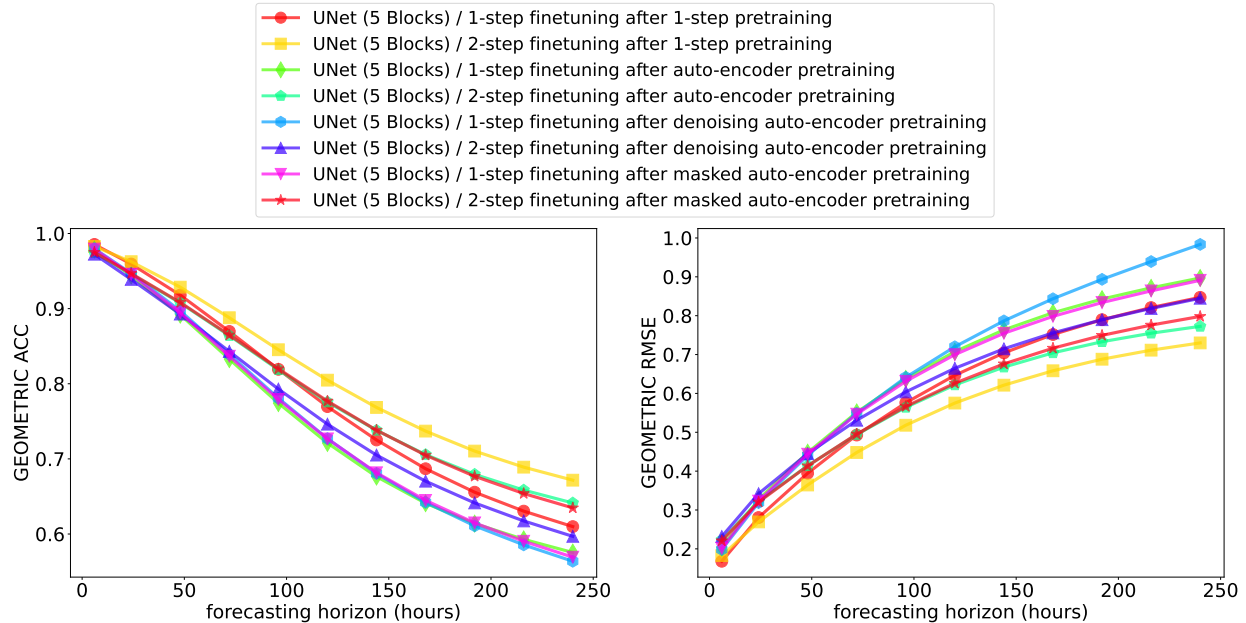


Figure 6: **Geometric ACC (left) and RMSE (right) for comparison of different pretraining objectives on UNet with 5 blocks.** The figure highlights that supervised pretraining achieves better performance in comparison to self-supervised pretraining using different objectives evaluated in this work (results in tabular form are presented in Table 5).

Note that since we do not use official implementation for all model classes, and use fixed hyperparameters, this may undermine the true performance of the model. We explore the efficacy of the multi-step fine-tuning as well as several other techniques that we introduce in subsequent sections for ResNet-50 with fully-convolutional decoder (Long et al., 2015) and Segformer (Xie et al., 2021) towards the end in Section 4.14.

### 4.3 Impact of self-supervised pretraining

A wide range of different pretraining objectives has been used for pretraining deep-learning models in the past (He et al., 2022; Brempong et al., 2022; El-Nouby et al., 2024). Man et al. (2023) applied mask-autoencoding objective (He et al., 2022) for the pretraining of weather-forecasting systems. However, their analysis confounded the impact of the pretraining objective, model architecture, and the training budget that our analysis attempts to disentangle. Similarly, ClimaX (Nguyen et al., 2023a) trained using heterogeneous sources, evading the possibility of understanding the marginal contribution of the pretraining objective itself. We explore the use of four simple pretraining techniques in this work:

- Pretraining directly on the forecasting task. Note that fine-tuning using this task is equivalent to training the model for longer with a restart in the learning rate schedule.
- Auto-encoder pretraining where the model is trained to reconstruct the input. In this formulation, we remove the skip connections as it introduces a trivial solution, and initialize these skip connections randomly in the fine-tuning phase.
- Masked auto-encoder (He et al., 2022) where we mask complete channels of the input, and

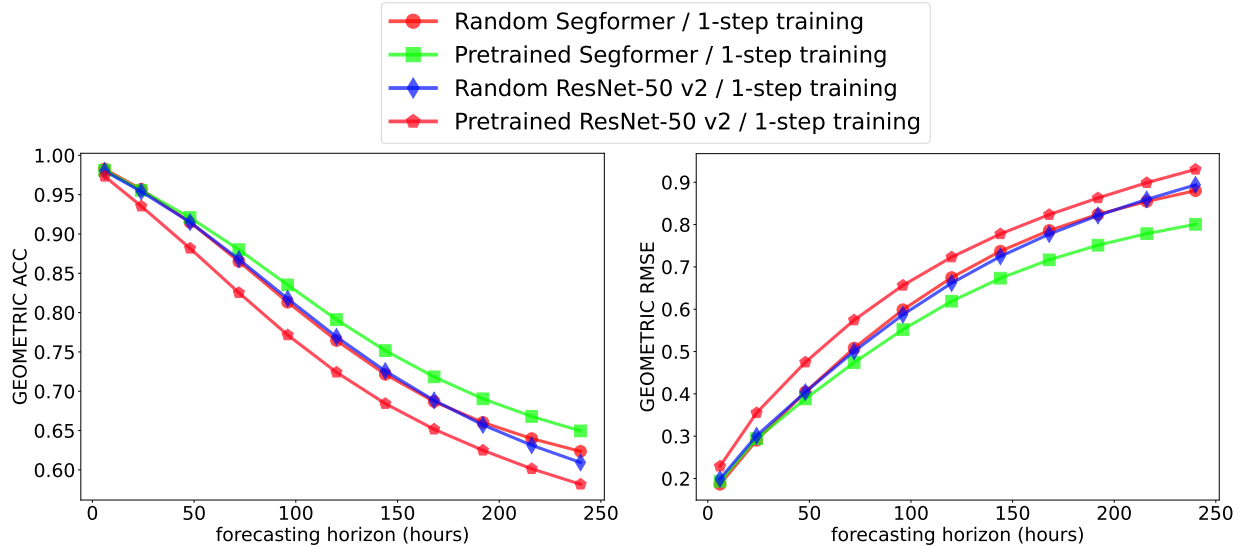


Figure 7: **Geometric ACC (left) and RMSE (right) when using image-based pretrained models.** The figure highlights that there are non-trivial gains for Segformer when using a pretrained model which was directly trained for segmentation as compared to ResNet-50 which was trained for classification (results in tabular form are presented in Table 6).

Model	Forecasting horizon (hours)										
	6	24	48	72	96	120	144	168	192	216	240
Random Segformer / 1-step training	<b>0.9825</b>	<b>0.9568</b>	0.9149	0.8650	0.8132	0.7645	0.7215	0.6869	0.6604	0.6398	0.6236
Pretrained Segformer / 1-step training	0.9811	0.9555	<b>0.9209</b>	<b>0.8800</b>	<b>0.8352</b>	<b>0.7911</b>	<b>0.7517</b>	<b>0.7183</b>	<b>0.6904</b>	<b>0.6680</b>	<b>0.6496</b>
Random ResNet-50 v2 / 1-step training	0.9801	0.9539	0.9150	0.8679	0.8177	0.7692	0.7257	0.6884	0.6572	0.6313	0.6094
Pretrained ResNet-50 v2 / 1-step training	0.9733	0.9353	0.8818	0.8253	0.7715	0.7241	0.6843	0.6517	0.6249	0.6014	0.5817

(a) Geometric ACC

Model	Forecasting horizon (hours)										
	6	24	48	72	96	120	144	168	192	216	240
Random Segformer / 1-step training	<b>0.1863</b>	<b>0.2902</b>	0.4044	0.5082	0.5988	0.6748	0.7372	0.7861	0.8240	0.8548	0.8802
Pretrained Segformer / 1-step training	0.1935	0.2942	<b>0.3882</b>	<b>0.4740</b>	<b>0.5520</b>	<b>0.6189</b>	<b>0.6734</b>	<b>0.7166</b>	<b>0.7513</b>	<b>0.7785</b>	<b>0.8007</b>
Random ResNet-50 v2 / 1-step training	0.1992	0.3012	0.4041	0.5006	0.5871	0.6618	0.7248	0.7774	0.8214	0.8594	0.8938
Pretrained ResNet-50 v2 / 1-step training	0.2292	0.3552	0.4748	0.5744	0.6564	0.7232	0.7779	0.8235	0.8629	0.8989	0.9304

(b) Geometric RMSE

Table 6: **Geometric ACC (a) and RMSE (b) when using image-based pretrained models.** The table highlights that there are non-trivial gains for Segformer when using a pretrained model which was directly trained for segmentation as compared to ResNet-50 which was trained for classification (results in graphical form are presented in Fig. 7).

apply the loss to reconstruct only the masked channels, following the masked auto-encoder recipe (He et al., 2022).

- Denoising auto-encoder (Bengio et al., 2013) where we add noise to the input, and ask the model to generate a denoised version of the input. In this case, since there is no trivial solution, we retain the skip connections in the model.

We always use the delta prediction task during fine-tuning, which may introduce a mismatch from the pretraining phase such as for the auto-encoder models. However, we assume that pretraining might still provide a useful initialization point for the model. We used a masking ratio of 50% for

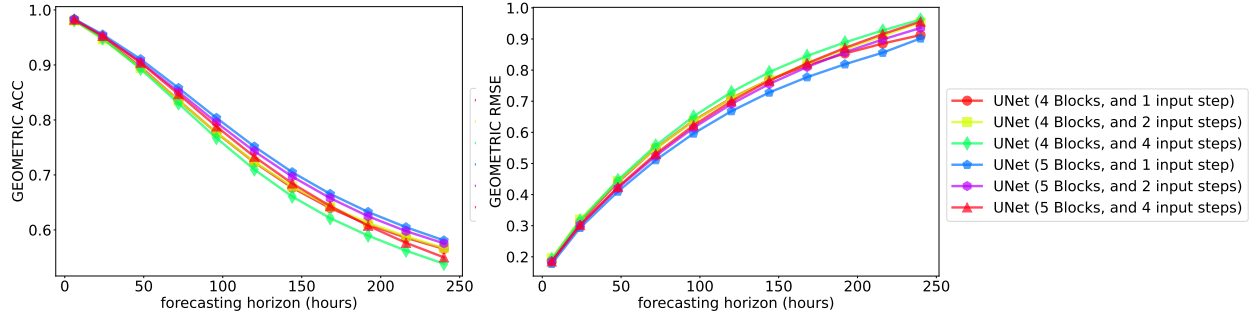


Figure 8: **Geometric ACC (left) and RMSE (right) with multi-step inputs.** Given the fixed number of training steps, we observe a negligible difference between 1 and 2 input steps starting with the next step prediction. However, performance significantly degrades when using 4 input steps despite achieving a similar starting performance to the 2 input step model for the next step i.e., 6h prediction (results in tabular form are presented in Table 7).

Model	Forecasting horizon (hours)										
	6	24	48	72	96	120	144	168	192	216	240
UNet (4 Blocks, and 1 input step)	0.9820	0.9495	0.8965	0.8360	0.7768	0.7228	0.6767	0.6398	0.6100	0.5858	0.5655
UNet (4 Blocks, and 2 input steps)	0.9806	0.9468	0.8942	0.8357	0.7773	0.7240	0.6791	0.6426	0.6129	0.5884	0.5673
UNet (4 Blocks, and 4 input steps)	0.9812	0.9481	0.8930	0.8300	0.7671	0.7098	0.6607	0.6214	0.5896	0.5623	0.5385
UNet (5 Blocks, and 1 input step)	<b>0.9838</b>	<b>0.9554</b>	<b>0.9105</b>	<b>0.8581</b>	<b>0.8038</b>	<b>0.7517</b>	<b>0.7050</b>	<b>0.6656</b>	<b>0.6327</b>	<b>0.6049</b>	<b>0.5809</b>
UNet (5 Blocks, and 2 input steps)	0.9825	0.9526	0.9055	0.8513	0.7954	0.7431	0.6969	0.6579	0.6248	0.5978	0.5755
UNet (5 Blocks, and 4 input steps)	0.9825	0.9528	0.9041	0.8470	0.7882	0.7332	0.6845	0.6434	0.6076	0.5766	0.5501

(a) Geometric ACC

Model	Forecasting horizon (hours)										
	6	24	48	72	96	120	144	168	192	216	240
UNet (4 Blocks, and 1 input step)	0.1871	0.3113	0.4397	0.5488	0.6376	0.7103	0.7689	0.8154	0.8535	0.8853	0.9127
UNet (4 Blocks, and 2 input steps)	0.1951	0.3196	0.4438	0.5480	0.6358	0.7092	0.7696	0.8208	0.8665	0.9096	0.9533
UNet (4 Blocks, and 4 input steps)	0.1922	0.3165	0.4467	0.5578	0.6515	0.7294	0.7936	0.8456	0.8892	0.9275	0.9625
UNet (5 Blocks, and 1 input step)	<b>0.1774</b>	<b>0.2933</b>	<b>0.4099</b>	<b>0.5109</b>	<b>0.5964</b>	<b>0.6683</b>	<b>0.7281</b>	<b>0.7773</b>	<b>0.8188</b>	<b>0.8561</b>	<b>0.9019</b>
UNet (5 Blocks, and 2 input steps)	0.1854	0.3020	0.4209	0.5244	0.6147	0.6911	0.7555	0.8100	0.8574	0.8984	0.9356
UNet (5 Blocks, and 4 input steps)	0.1851	0.3019	0.4240	0.5306	0.6224	0.7001	0.7660	0.8218	0.8713	0.9158	0.9559

(b) Geometric RMSE

Table 7: **Geometric ACC (a) and RMSE (b) with multi-step inputs.** Given the fixed number of training steps, we observe a negligible difference between 1 and 2 input steps starting with the next step prediction. However, performance significantly degrades when using 4 input steps despite achieving a similar starting performance to the 2 input step model for the next step i.e., 6h prediction (results in graphical form are presented in Fig. 8).

masked auto-encoder training and a standard deviation of 0.1 for noise injection for the training of denoising auto-encoder.

### 4.3.1 UNet (4 Blocks)

The geometric ACC and RMSE for the different pretraining objectives on 4-block UNet are presented in Table 4 (Fig. 5). The results highlight that pretraining using the supervised objective (pretraining and fine-tuning tasks are the same in this case) achieves better performance in comparison to the evaluated self-supervised objectives. Despite not observing gains in performance with self-supervised objectives in our case, it is likely that improvements in the objectives used would result in significant improvement in forecasting capabilities in the future. Furthermore, we only evaluate a single set

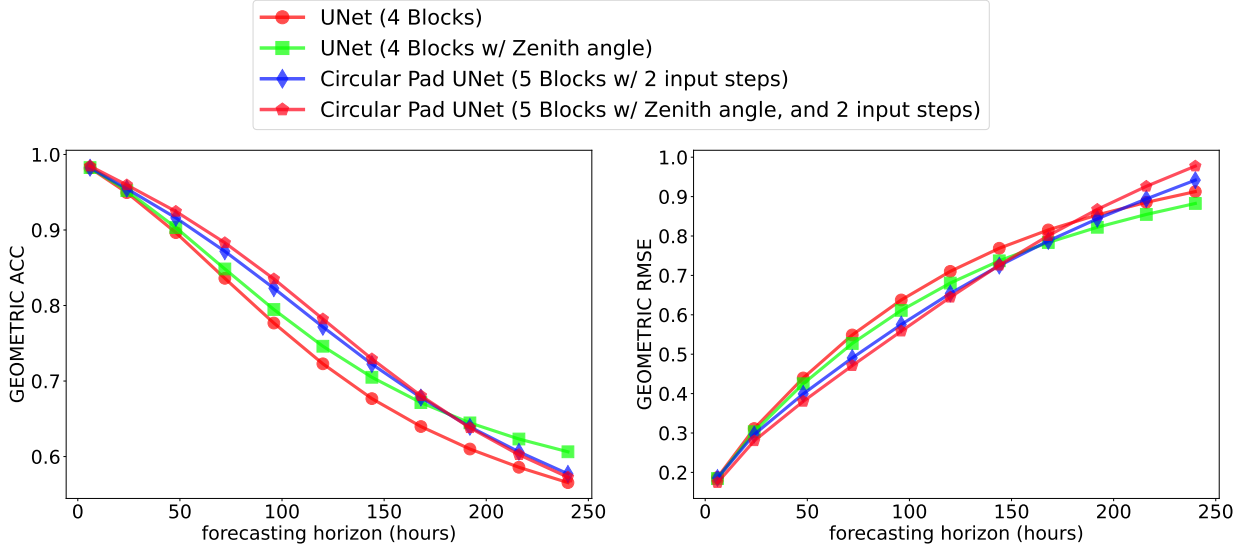


Figure 9: **Geometric ACC (left) and RMSE (right) with the inclusion of zenith angle.** The figure highlights that the Zenith angle provides consistent gains in predictive performance at both short-horizon and long-horizon forecasts (results in tabular form are presented in Table 8).

Model	Forecasting horizon (hours)										
	6	24	48	72	96	120	144	168	192	216	240
UNet (4 Blocks)	0.9820	0.9495	0.8965	0.8360	0.7768	0.7228	0.6767	0.6398	0.6100	0.5858	0.5655
UNet (4 Blocks w/ Zenith angle)	0.9826	0.9521	0.9032	0.8484	0.7947	0.7461	0.7050	0.6715	<b>0.6446</b>	<b>0.6232</b>	<b>0.6063</b>
Circular Pad UNet (5 Blocks w/ 2 input steps)	0.9824	0.9547	0.9161	0.8718	0.8229	0.7717	0.7224	0.6781	0.6393	0.6063	0.5771
Circular Pad UNet (5 Blocks w/ Zenith angle, and 2 input steps)	<b>0.9846</b>	<b>0.9597</b>	<b>0.9246</b>	<b>0.8831</b>	<b>0.8352</b>	<b>0.7822</b>	<b>0.7293</b>	<b>0.6806</b>	0.6381	0.6025	0.5727

(a) Geometric ACC

Model	Forecasting horizon (hours)										
	6	24	48	72	96	120	144	168	192	216	240
UNet (4 Blocks)	0.1871	0.3113	0.4397	0.5488	0.6376	0.7103	0.7689	0.8154	0.8535	0.8853	0.9127
UNet (4 Blocks w/ Zenith angle)	0.1844	0.3033	0.4250	0.5272	0.6113	0.6805	0.7370	<b>0.7835</b>	<b>0.8222</b>	<b>0.8547</b>	<b>0.8826</b>
Circular Pad UNet (5 Blocks w/ 2 input steps)	0.1858	0.2962	0.3993	0.4905	0.5753	0.6541	<b>0.7248</b>	0.7874	0.8436	0.8942	0.9418
Circular Pad UNet (5 Blocks w/ Zenith angle, and 2 input steps)	<b>0.1740</b>	<b>0.2801</b>	<b>0.3802</b>	<b>0.4709</b>	<b>0.5584</b>	<b>0.6445</b>	0.7259	0.8007	0.8676	0.9261	0.9774

(b) Geometric RMSE

Table 8: **Geometric ACC (a) and RMSE (b) with the inclusion of zenith angle.** The table highlights that the Zenith angle provides consistent gains in predictive performance at both short-horizon and long-horizon forecasts (results in graphical form are presented in Fig. 9).

of hyperparameters. It is possible that a slightly different combination of these hyperparameters can introduce significant differences in these results. We leave the evaluation of other pretraining techniques such as generative pretraining (Chen et al., 2020), as well as a more thorough search over hyperparameters as promising directions to explore in the future.

### 4.3.2 UNet (5 Blocks)

The geometric ACC and RMSE for the different pretraining objectives on 5-block UNet are presented in Table 5 (Fig. 6). These results are consistent with the results on the 4-block UNet, where we observe supervised pretraining to outperform self-supervised objectives.

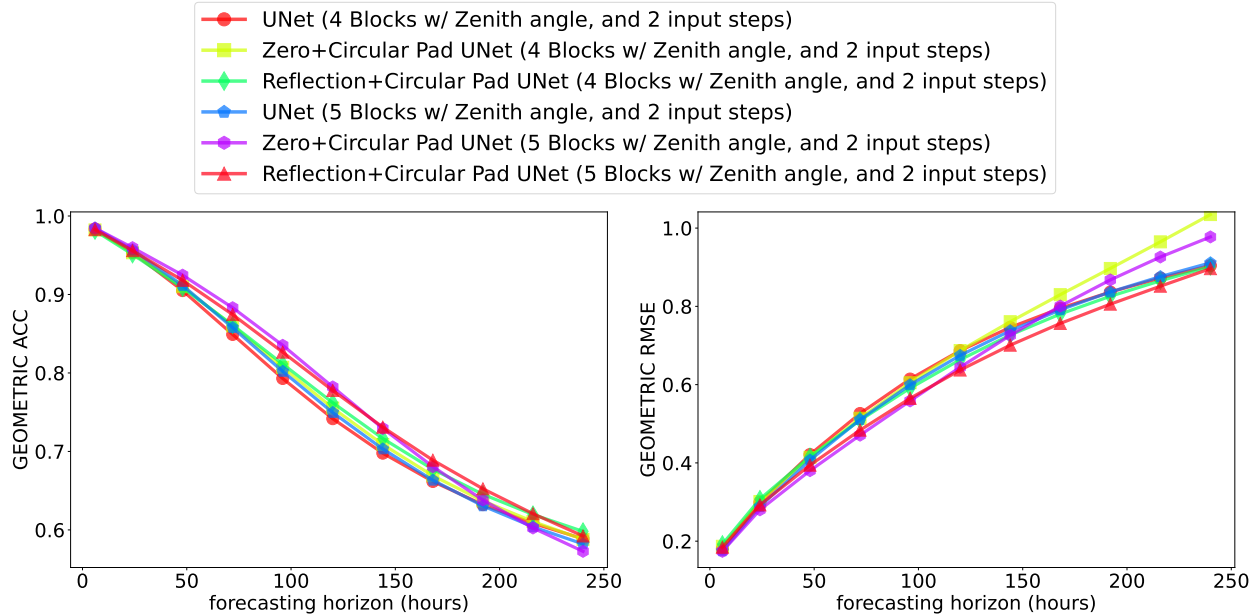


Figure 10: **Geometric ACC (a) and RMSE (b) with different padding schemes for the convolutional layers in the UNet architecture.** The figure highlights that using circular padding along the longitudinal direction and either zero or reflection padding along the latitudinal direction provides consistent gains in performance (results in tabular form are presented in Table 9).

#### 4.4 Impact of using image-based pretraining

Weather models process different resolutions and channels in contrast to their image-based counterparts. Despite this, image-based pretraining has been looked at as a form of careful initialization that is useful even in the presence of a task mismatch (Kolesnikov et al., 2020; Bommasani et al., 2021).

Therefore, we aim to evaluate the impact of using pretrained weights obtained after image-based pretraining and finetune them for the weather forecasting task by reinitializing the first and the last layer to match the input and output channels. Note that not all parameters are loaded i.e., some parameters are initialized randomly such as the decoder head that we attach to the original model. This includes the input and output features as the image models are trained with just 3 input channels, while we have a significantly larger number of channels in our case. In particular, we use the Segformer B5<sup>5</sup> pretrained backbone from MMSeg as our Segformer pretrained model and use the torchvision pretrained ResNet-50<sup>6</sup> (He et al., 2016) as our ResNet-50 with conv-decoder pretrained model (which is only trained for classification).

The geometric ACC and RMSE for image-based pretraining are presented in Table 6 (Fig. 7). There is a conflicting trend where we see performance improvement for the Segformer model while we observe performance degradation for ResNet-50. We consider this to be primarily an artifact of the loaded model as only the base residual modules were successfully loaded for ResNet-50, leaving the decoder as well as the input stem to be initialized randomly. Furthermore, the model is only trained for classification as compared to Segformer, which is trained directly for segmentation. It would be interesting as a future step to train perfectly aligned models (except the input and the output layers which would be different) and redo this evaluation to get a clear sense of the transfer

<sup>5</sup>[https://download.openmmlab.com/mmssegmentation/v0.5/pretrain/segformer/mit\\_b5\\_20220624-658746d9.pth](https://download.openmmlab.com/mmssegmentation/v0.5/pretrain/segformer/mit_b5_20220624-658746d9.pth)

<sup>6</sup><https://download.pytorch.org/models/resnet50-11ad3fa6.pth>

Model	Forecasting horizon (hours)										
	6	24	48	72	96	120	144	168	192	216	240
UNet (4 Blocks w/ Zenith angle, and 2 input steps)	0.9834	0.9536	0.9049	0.8490	0.7929	0.7417	0.6978	0.6617	0.6322	0.6084	0.5887
Zero+Circular Pad UNet (4 Blocks w/ Zenith angle, and 2 input steps)	0.9823	0.9531	0.9099	0.8601	0.8071	0.7553	0.7089	0.6690	0.6370	0.6107	0.5880
Reflection+Circular Pad UNet (4 Blocks w/ Zenith angle, and 2 input steps)	0.9812	0.9511	0.9084	0.8610	0.8114	0.7621	0.7165	0.6772	0.6454	0.6196	<b>0.5981</b>
UNet (5 Blocks w/ Zenith angle, and 2 input steps)	0.9844	0.9569	0.9115	0.8577	0.8020	0.7496	0.7031	0.6633	0.6306	0.6039	0.5821
Zero+Circular Pad UNet (5 Blocks w/ Zenith angle, and 2 input steps)	<b>0.9846</b>	<b>0.9597</b>	<b>0.9246</b>	<b>0.8831</b>	<b>0.8352</b>	<b>0.7822</b>	0.7293	0.6806	0.6381	0.6025	0.5727
Reflection+Circular Pad UNet (5 Blocks w/ Zenith angle, and 2 input steps)	0.9827	0.9558	0.9180	0.8744	0.8265	0.7777	<b>0.7309</b>	<b>0.6889</b>	<b>0.6524</b>	<b>0.6207</b>	0.5923

(a) Geometric ACC

Model	Forecasting horizon (hours)										
	6	24	48	72	96	120	144	168	192	216	240
UNet (4 Blocks w/ Zenith angle, and 2 input steps)	0.1808	0.2990	0.4214	0.5263	0.6143	0.6870	0.7462	0.7950	0.8366	0.8723	0.9043
Zero+Circular Pad UNet (4 Blocks w/ Zenith angle, and 2 input steps)	0.1869	0.3014	0.4141	0.5141	0.6049	0.6870	0.7608	0.8299	0.8968	0.9648	1.0346
Reflection+Circular Pad UNet (4 Blocks w/ Zenith angle, and 2 input steps)	0.1922	0.3076	0.4161	0.5091	0.5910	0.6636	0.7267	0.7804	0.8258	0.8652	0.9017
UNet (5 Blocks w/ Zenith angle, and 2 input steps)	0.1751	0.2885	0.4072	0.5108	0.5996	0.6747	0.7376	0.7911	0.8367	0.8760	0.9112
Zero+Circular Pad UNet (5 Blocks w/ Zenith angle, and 2 input steps)	<b>0.1740</b>	<b>0.2801</b>	<b>0.3802</b>	<b>0.4709</b>	<b>0.5584</b>	0.6445	0.7259	0.8007	0.8676	0.9261	0.9774
Reflection+Circular Pad UNet (5 Blocks w/ Zenith angle, and 2 input steps)	0.1845	0.2927	0.3942	0.4837	0.5649	<b>0.6372</b>	<b>0.7008</b>	<b>0.7563</b>	<b>0.8056</b>	<b>0.8515</b>	<b>0.8963</b>

(b) Geometric RMSE

Table 9: **Geometric ACC (a) and RMSE (b) with different padding schemes for the convolutional layers in the UNet architecture.** The table highlights that using circular padding along the longitudinal direction and either zero or reflection padding along the latitudinal direction provides consistent gains in performance (results in graphical form are presented in Fig. 10).

Model	Forecasting horizon (hours)										
	6	24	48	72	96	120	144	168	192	216	240
Circular Pad UNet (4 Blocks w/ Zenith angle, and 2 input steps)	0.9823	0.9531	0.9099	0.8601	0.8071	0.7553	0.7089	0.6690	0.6370	0.6107	0.5880
Circular Pad UNet (4 Blocks w/ Zenith angle, 2 input steps, and Gaussian noise $\sigma = 0.05$ )	0.9808	0.9498	0.9054	0.8560	0.8049	0.7553	0.7108	0.6722	0.6398	0.6116	0.5858
Circular Pad UNet (4 Blocks w/ Zenith angle, 2 input steps, and Perlin noise $\sigma = 0.05$ )	0.9828	0.9540	0.9102	0.8588	0.8043	0.7505	0.7019	0.6609	0.6269	0.5979	0.5739
Circular Pad UNet (5 Blocks w/ Zenith angle, and 2 input steps)	<b>0.9846</b>	<b>0.9597</b>	<b>0.9246</b>	<b>0.8831</b>	<b>0.8352</b>	<b>0.7822</b>	0.7293	0.6806	0.6381	0.6025	0.5727
Circular Pad UNet (5 Blocks w/ Zenith angle, 2 input steps, and Gaussian noise $\sigma = 0.05$ )	0.9821	0.9542	0.9156	0.8710	0.8219	0.7717	0.7247	0.6829	0.6472	0.6167	0.5902
Circular Pad UNet (5 Blocks w/ Zenith angle, 2 input steps, and Perlin noise $\sigma = 0.05$ )	0.9840	0.9583	0.9219	0.8792	0.8315	0.7814	<b>0.7340</b>	<b>0.6914</b>	<b>0.6558</b>	<b>0.6273</b>	<b>0.6038</b>

Model	Forecasting horizon (hours)										
	6	24	48	72	96	120	144	168	192	216	240
Circular Pad UNet (4 Blocks w/ Zenith angle, and 2 input steps)	0.1869	0.3014	0.4141	0.5141	0.6049	0.6870	0.7608	0.8299	0.8968	0.9648	1.0346
Circular Pad UNet (4 Blocks w/ Zenith angle, 2 input steps, and Gaussian noise $\sigma = 0.05$ )	0.1939	0.3116	0.4233	0.5202	0.6074	0.6866	0.7576	0.8222	0.8827	0.9421	1.0023
Circular Pad UNet (4 Blocks w/ Zenith angle, 2 input steps, and Perlin noise $\sigma = 0.05$ )	0.1841	0.2986	0.4111	0.5105	0.5983	0.6757	0.7417	0.7974	0.8461	0.8915	0.9354
Circular Pad UNet (5 Blocks w/ Zenith angle, and 2 input steps)	<b>0.1740</b>	<b>0.2801</b>	<b>0.3802</b>	<b>0.4709</b>	<b>0.5584</b>	0.6445	0.7259	0.8007	0.8676	0.9261	0.9774
Circular Pad UNet (5 Blocks w/ Zenith angle, 2 input steps, and Gaussian noise $\sigma = 0.05$ )	0.1871	0.2981	0.4006	0.4908	0.5734	0.6472	0.7110	0.7661	0.8140	0.8571	0.8974
Circular Pad UNet (5 Blocks w/ Zenith angle, 2 input steps, and Perlin noise $\sigma = 0.05$ )	0.1774	0.2848	0.3863	0.4773	0.5616	<b>0.6390</b>	<b>0.7063</b>	<b>0.7636</b>	<b>0.8109</b>	<b>0.8494</b>	<b>0.8825</b>

(a) Geometric RMSE

Table 10: **Geometric ACC (a) and RMSE (b) with different noise addition schemes.** The table highlights that adding some forms of noise (particularly Perlin noise as used in prior work (Bi et al., 2022; Chen et al., 2023)) improves predictive performance for the long-horizon case with only minor detrimental effects on the short-horizon forecast (results in graphical form are presented in Fig. 11).

possible with image-based pretrained models.

## 4.5 Impact of multi-step inputs

All our prior comparisons just took a single step as input. However, it is possible to condition the model prediction on multiple previous input steps as commonly done in the past (Lam et al., 2022; Price et al., 2023; Chen et al., 2023). This is particularly useful when doing long auto-regressive rollouts where the model can look at the previous steps to decide the right delta to be used for the next step. The problem formulation in this case is  $\mathbf{s}_t = \mathbf{s}_{t-1} + \Phi(\{\mathbf{s}_{t-n}, \dots, \mathbf{s}_{t-2}, \mathbf{s}_{t-1}\})$  where  $n$  specifies the number of input time-steps.

The geometric ACC and RMSE for multi-step inputs are presented in Table 7 (Fig. 8). These results highlight that model performance is nearly maintained for 1 or 2 input steps but degrades significantly when using 4 input steps. We consider the difference in performance between the 1 and

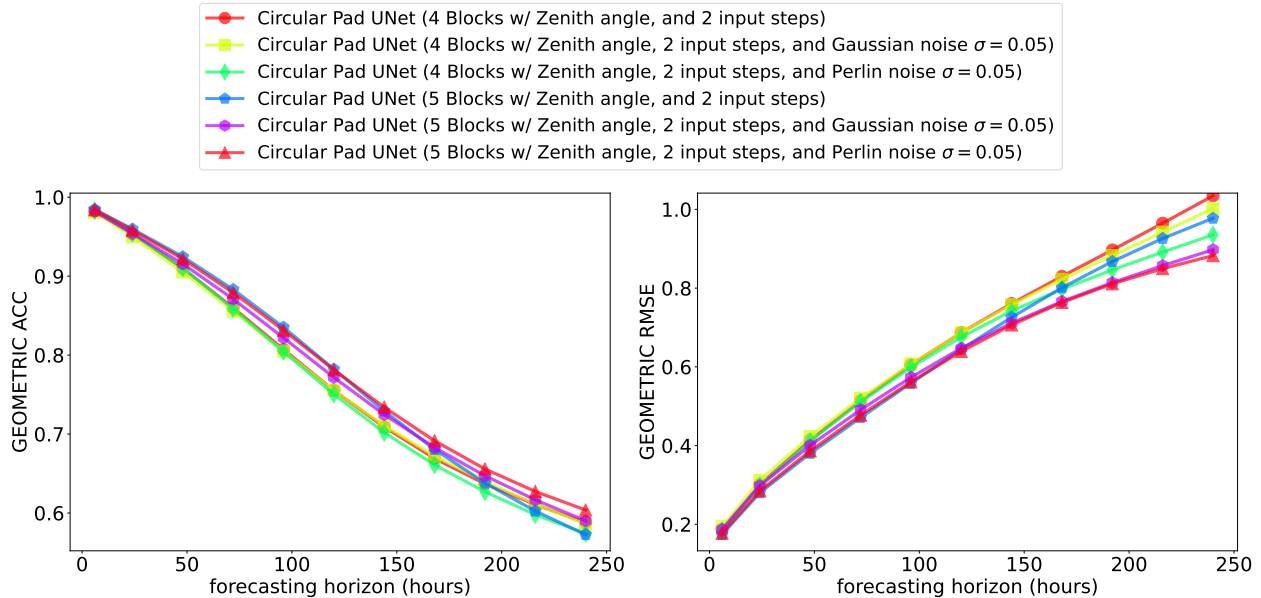


Figure 11: **Geometric ACC (left) and RMSE (right) with different noise addition schemes.** The figure highlights that adding some forms of noise (particularly Perlin noise as used in prior work (Bi et al., 2022; Chen et al., 2023)) improves predictive performance for the long-horizon case with only minor detrimental effects on the short-horizon forecast (results in tabular form are presented in Table 10).

Model	Forecasting horizon (hours)										
	6	24	48	72	96	120	144	168	192	216	240
Circular Pad UNet (4 Blocks w/ Zenith angle, and 2 input steps)	0.9823	0.9531	0.9099	0.8601	0.8071	0.7553	0.7089	0.6690	0.6370	0.6107	0.5880
Circular Pad UNet (4 Blocks w/ Zenith angle, 2 input steps, and Input loc)	0.9806	0.9497	0.9051	0.8552	0.8030	0.7522	0.7067	0.6678	0.6357	0.6085	0.5852
Circular Pad UNet (5 Blocks w/ Zenith angle, and 2 input steps)	<b>0.9846</b>	<b>0.9597</b>	<b>0.9246</b>	<b>0.8831</b>	<b>0.8352</b>	<b>0.7822</b>	0.7293	0.6806	0.6381	0.6025	0.5727
Circular Pad UNet (5 Blocks w/ Zenith angle, 2 input steps, and Input loc)	0.9826	0.9557	0.9184	0.8755	0.8279	0.7788	<b>0.7325</b>	<b>0.6913</b>	<b>0.6558</b>	<b>0.6247</b>	<b>0.5977</b>

(a) Geometric ACC

Model	Forecasting horizon (hours)										
	6	24	48	72	96	120	144	168	192	216	240
Circular Pad UNet (4 Blocks w/ Zenith angle, and 2 input steps)	0.1869	0.3014	0.4141	0.5141	0.6049	0.6870	0.7608	0.8299	0.8968	0.9648	1.0346
Circular Pad UNet (4 Blocks w/ Zenith angle, 2 input steps, and Input loc)	0.1948	0.3114	0.4210	0.5136	0.5941	0.6633	0.7207	<b>0.7687</b>	<b>0.8096</b>	<b>0.8464</b>	<b>0.8811</b>
Circular Pad UNet (5 Blocks w/ Zenith angle, and 2 input steps)	<b>0.1740</b>	<b>0.2801</b>	<b>0.3802</b>	<b>0.4709</b>	<b>0.5584</b>	0.6445	0.7259	0.8007	0.8676	0.9261	0.9774
Circular Pad UNet (5 Blocks w/ Zenith angle, 2 input steps, and Input loc)	0.1848	0.2931	0.3934	0.4827	0.5660	<b>0.6425</b>	<b>0.7099</b>	0.7692	0.8223	0.8715	0.9179

(b) Geometric RMSE

Table 11: **Geometric ACC (a) and RMSE (b) with the addition of 3D coordinates on the sphere as static masks.** The figure table that providing the model with this auxiliary information regarding the proximity of different points on the globe results in more stable long-horizon forecasts (results in graphical form are presented in Fig. 12).

2 steps an artifact of the performance difference at the first step as evident by the constant difference between the model outputs. Note that we are using delta prediction formulation, where we add the predicted delta to the last input step, which might reduce the utility of the inclusion of previous steps in contrast to direct prediction. Furthermore, multiple input steps when combined with other techniques such as a longer training schedule might outperform the single-step performance. As the performance degrades significantly with 4 input steps, we use two input steps for all subsequent experiments unless mentioned otherwise.

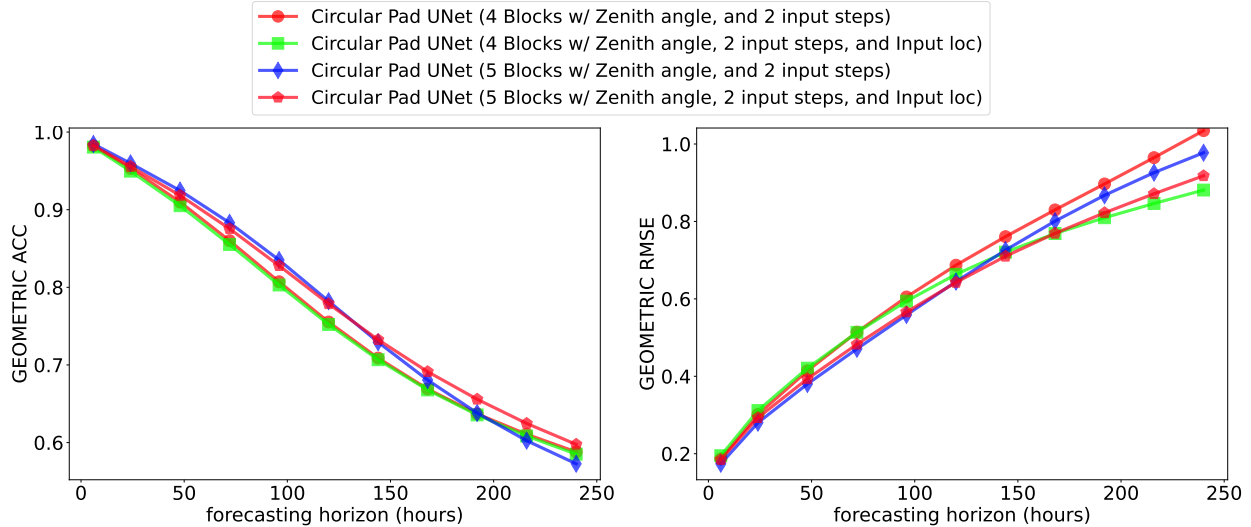


Figure 12: **Geometric ACC (left) and RMSE (right) with the addition of 3D coordinates on the sphere as static masks.** The figure highlights that providing the model with this auxiliary information regarding the proximity of different points on the globe results in more stable long-horizon forecasts (results in tabular form are presented in Table 11).

Model	Forecasting horizon (hours)										
	6	24	48	72	96	120	144	168	192	216	240
Circular Pad UNet (4 Blocks w/ Zenith angle, 2 input steps, and MSE loss)	0.9823	0.9531	0.9099	0.8601	0.8071	0.7553	0.7089	0.6690	0.6370	0.6107	0.5880
Circular Pad UNet (4 Blocks w/ Zenith angle, 2 input steps, and L1 loss)	0.9761	0.9419	0.8998	0.8548	0.8076	0.7609	0.7186	0.6842	0.6562	0.6324	0.6125
Circular Pad UNet (4 Blocks w/ Zenith angle, 2 input steps, and Geometric MSE loss)	0.9830	0.9538	0.9111	0.8619	0.8093	0.7568	0.7092	0.6677	0.6330	0.6039	0.5787
Circular Pad UNet (4 Blocks w/ Zenith angle, 2 input steps, and Geometric L1 loss)	0.9787	0.9467	0.9060	0.8622	0.8157	<b>0.7688</b>	<b>0.7265</b>	<b>0.6914</b>	<b>0.6631</b>	<b>0.6401</b>	<b>0.6211</b>
Circular Pad UNet (4 Blocks w/ Zenith angle, 2 input steps, and Huber loss)	0.9812	0.9505	0.9078	0.8589	0.8072	0.7564	0.7114	0.6746	0.6460	0.6222	0.6016
Circular Pad UNet (4 Blocks w/ Zenith angle, 2 input steps, and L1-L2 loss)	<b>0.9834</b>	<b>0.9556</b>	<b>0.9155</b>	<b>0.8690</b>	<b>0.8185</b>	0.7669	0.7192	0.6789	0.6469	0.6206	0.5976

(a) Geometric ACC

Model	Forecasting horizon (hours)										
	6	24	48	72	96	120	144	168	192	216	240
Circular Pad UNet (4 Blocks w/ Zenith angle, 2 input steps, and MSE loss)	0.1869	0.3014	0.4141	0.5141	0.6049	0.6870	0.7608	0.8299	0.8968	0.9648	1.0346
Circular Pad UNet (4 Blocks w/ Zenith angle, 2 input steps, and L1 loss)	0.2198	0.3403	0.4395	0.5231	0.5980	0.6646	0.7210	0.7658	0.8030	0.8356	0.8644
Circular Pad UNet (4 Blocks w/ Zenith angle, 2 input steps, and Geometric MSE loss)	0.1828	0.2980	0.4093	0.5076	0.5962	0.6758	0.7444	0.8043	0.8566	0.9043	0.9506
Circular Pad UNet (4 Blocks w/ Zenith angle, 2 input steps, and Geometric L1 loss)	0.2078	0.3247	0.4243	0.5089	0.5860	<b>0.6555</b>	<b>0.7137</b>	<b>0.7600</b>	<b>0.7973</b>	<b>0.8281</b>	<b>0.8555</b>
Circular Pad UNet (4 Blocks w/ Zenith angle, 2 input steps, and Huber loss)	0.1924	0.3099	0.4189	0.5145	0.5989	0.6721	0.7329	0.7826	0.8243	0.8627	0.9004
Circular Pad UNet (4 Blocks w/ Zenith angle, 2 input steps, and L1-L2 loss)	<b>0.1810</b>	<b>0.2933</b>	<b>0.4005</b>	<b>0.4956</b>	<b>0.5818</b>	0.6593	0.7259	0.7815	0.8268	0.8663	0.9037

(b) Geometric RMSE

Table 12: **Geometric ACC (a) and RMSE (b) with the use of different loss functions on 4-block UNet.** The table highlights that variants of  $L_1$  loss, including  $L_1$ , geometric  $L_1$ ,  $L_1-L_2$ , and Huber loss, provide consistent gains in predictive performance in contrast to MSE, potentially due to their robustness against outliers (results in graphical form are presented in Fig. 13).

## 4.6 Impact of zenith angle

Solar zenith angle specifies the angle of the Sun to the vertical, providing a notion of time to the model. Therefore, this has been commonly used in prior models (Pathak et al., 2022). We also evaluate the impact of adding zenith angle as an additional input channel to the model. For the auto-regressive rollout, we append the next zenith angle to the model’s prediction before feeding it back to the model. We only add the zenith angle for the last input step, even when using multi-step inputs as the delta is computed w.r.t. the last input step.

The geometric ACC and RMSE for zenith angle comparison are presented in Table 8 (Fig. 9). It is clear from the results that the zenith angle always improves performance for both short-horizon

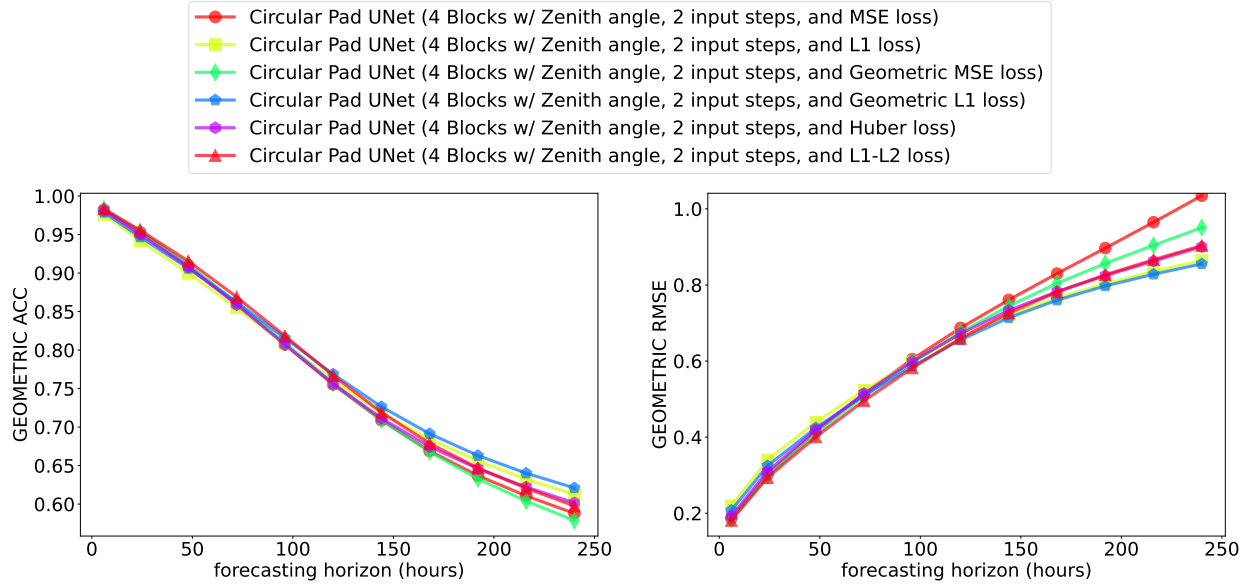


Figure 13: **Geometric ACC (left) and RMSE (right) with the use of different loss functions on 4-block UNet.** The figure highlights that variants of  $L_1$  loss, including  $L_1$ , geometric  $L_1$ ,  $L_1-L_2$ , and Huber loss, provide consistent gains in predictive performance in contrast to MSE, potentially due to their robustness against outliers (results in tabular form are presented in Table 12).

Model	Forecasting horizon (hours)										
	6	24	48	72	96	120	144	168	192	216	240
Circular Pad UNet (5 Blocks w/ Zenith angle, 2 input steps, and MSE loss)	<b>0.9846</b>	<b>0.9597</b>	<b>0.9246</b>	<b>0.8831</b>	<b>0.8352</b>	0.7822	0.7293	0.6806	0.6381	0.6025	0.5727
Circular Pad UNet (5 Blocks w/ Zenith angle, 2 input steps, and L1 loss)	0.9783	0.9480	0.9118	0.8720	0.8274	0.7807	0.7363	0.6976	0.6659	<b>0.6403</b>	<b>0.6189</b>
Circular Pad UNet (5 Blocks w/ Zenith angle, 2 input steps, and Geometric MSE loss)	<b>0.9846</b>	0.9591	0.9223	0.8789	0.8304	0.7799	0.7319	0.6891	0.6529	0.6222	0.5959
Circular Pad UNet (5 Blocks w/ Zenith angle, 2 input steps, and Geometric L1 loss)	0.9802	0.9510	0.9138	0.8722	0.8263	0.7788	0.7338	0.6951	0.6624	0.6352	0.6120
Circular Pad UNet (5 Blocks w/ Zenith angle, 2 input steps, and Huber loss)	0.9839	0.9581	0.9224	0.8807	0.8345	<b>0.7870</b>	<b>0.7422</b>	<b>0.7024</b>	<b>0.6672</b>	0.6358	0.6079
Circular Pad UNet (5 Blocks w/ Zenith angle, 2 input steps, and L1-L2 loss)	0.9841	0.9591	0.9239	0.8822	0.8351	0.7847	0.7358	0.6938	0.6579	0.6279	0.6019

(a) Geometric ACC

Model	Forecasting horizon (hours)										
	6	24	48	72	96	120	144	168	192	216	240
Circular Pad UNet (5 Blocks w/ Zenith angle, 2 input steps, and MSE loss)	0.1740	<b>0.2801</b>	<b>0.3802</b>	<b>0.4709</b>	0.5584	0.6445	0.7259	0.8007	0.8676	0.9261	0.9774
Circular Pad UNet (5 Blocks w/ Zenith angle, 2 input steps, and L1 loss)	0.2092	0.3219	0.4141	0.4951	0.5722	0.6440	0.7069	0.7597	0.8031	<b>0.8393</b>	<b>0.8710</b>
Circular Pad UNet (5 Blocks w/ Zenith angle, 2 input steps, and Geometric MSE loss)	<b>0.1736</b>	0.2816	0.3856	0.4788	0.5650	0.6436	0.7135	0.7751	0.8301	0.8840	0.9417
Circular Pad UNet (5 Blocks w/ Zenith angle, 2 input steps, and Geometric L1 loss)	0.2001	0.3106	0.4070	0.4923	0.5724	0.6460	0.7108	0.7654	0.8123	0.8529	0.8899
Circular Pad UNet (5 Blocks w/ Zenith angle, 2 input steps, and Huber loss)	0.1784	0.2853	0.3853	0.4746	<b>0.5568</b>	<b>0.6305</b>	<b>0.6940</b>	<b>0.7483</b>	<b>0.7962</b>	0.8402	0.8825
Circular Pad UNet (5 Blocks w/ Zenith angle, 2 input steps, and L1-L2 loss)	0.1767	0.2821	0.3826	0.4748	0.5623	3.3412	457.1086	2498.2460	12190.9917	58497.4833	279300.7111

(b) Geometric RMSE

Table 13: **Geometric ACC (a) and RMSE (b) with the use of different loss functions on 5-block UNet.** In contrast to the 4-block UNet, MSE dominates in the short-horizon prediction, while variants of  $L_1$  loss dominates in the long-horizon prediction (results in tabular form are presented in Fig. 14).

and long-horizon predictions by equipping the model with a notion of time. Hence, all our subsequent models use the zenith angle unless mentioned otherwise.

#### 4.7 Impact of padding scheme

We evaluated the impact of different padding schemes. The default UNet padding scheme is zero padding on both sides. As we have continuity along the longitudinal direction (x-axis), we also evaluate the impact of using a circular padding scheme in the longitudinal direction. Furthermore,

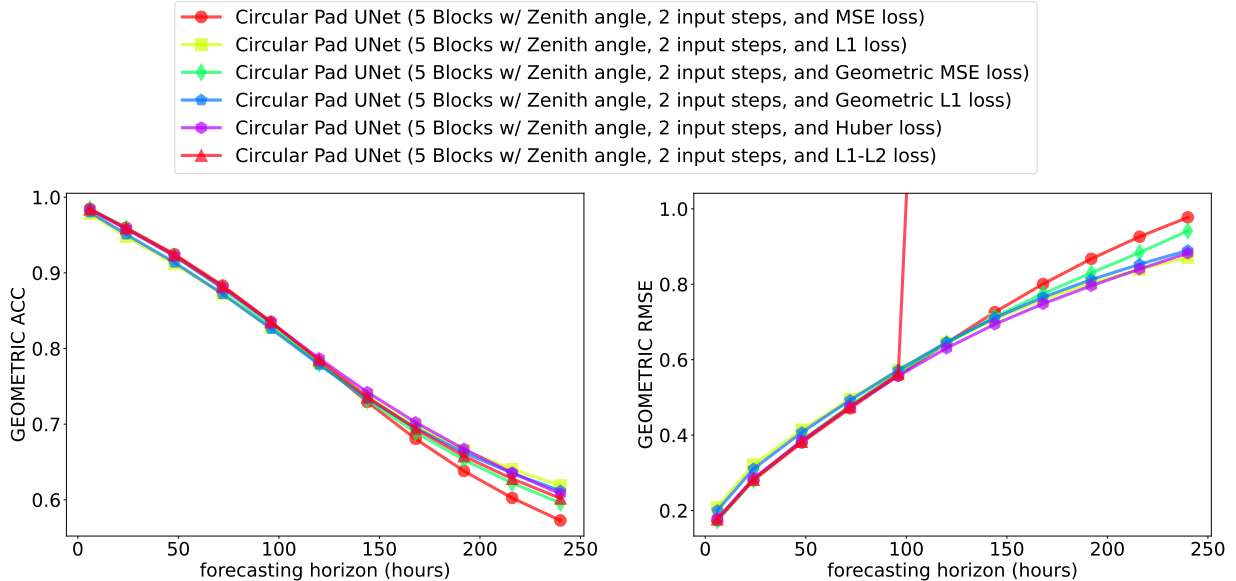


Figure 14: **Geometric ACC (left) and RMSE (right) with the use of different loss functions on 5-block UNet.** In contrast to the 4-block UNet, MSE dominates in the short-horizon prediction, while variants of  $L_1$  loss dominate in the long-horizon prediction (results in tabular form are presented in Table 13).

we evaluate the impact of adding the reflection padding scheme instead of the zero padding scheme for the latitudinal direction (y-axis) to account for the Neumann boundary condition. McCabe et al. (2023) explored sphere-to-torus transform as a way to stabilize auto-regressive rollouts for operator-based models (Pathak et al., 2022). Recently, Cheon et al. (2024) also explored using a circular padding scheme. However, they do not disentangle the marginal contribution of the padding scheme itself, which is a focus of our work.

The geometric ACC and RMSE for different padding schemes are presented in Table 9 (Fig. 10). We do see a clear improvement when considering longer prediction horizons with circular padding along the longitudinal direction, which encodes the information regarding the geometry of the sphere. We also see significant differences in performance when replacing zero padding with reflection padding along the latitudinal direction. We consider simple ways to encode geometric information about the sphere within the model to be an exciting direction for further research. We use circular padding along the longitudinal direction and zero padding along the latitudinal direction for all further experiments unless mentioned otherwise.

#### 4.8 Impact of noise addition

Noise addition has been used as an effective strategy for ensemble generation in the past (Pathak et al., 2022; Bi et al., 2022), where FourCastNet (Pathak et al., 2022) added Gaussian noise while Pangu-weather (Bi et al., 2022) and FuXi (Chen et al., 2023) applied Perlin noise (Perlin, 2002) to the initial states. Given these evaluations, it is useful to understand the impact of noise addition on model performance during training as a regularization technique (Lopes et al., 2019). Therefore, we evaluate the impact of additive Gaussian and Perlin noise during model training.

The geometric ACC and RMSE for noise addition are presented in Table 10 (Fig. 11). The figure highlights that adding noise improves model performance in the long-horizon prediction

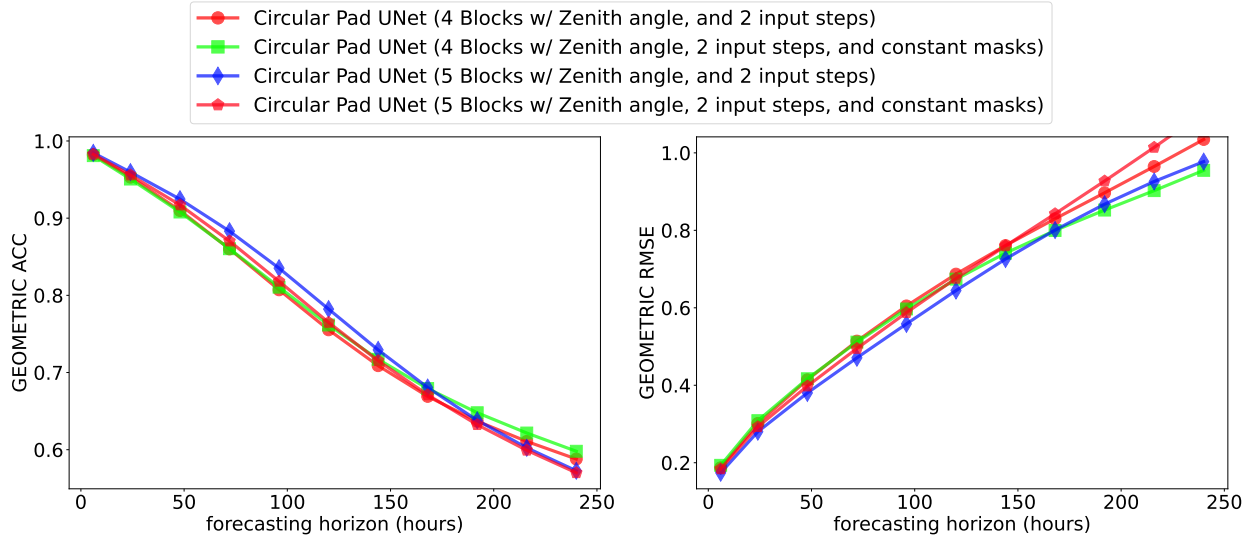


Figure 15: **Geometric ACC (left) and RMSE (right) with the addition of static constant masks including topography, soil-type, and land-sea mask following (Bi et al., 2022).** The figure highlights an interesting trend where the performance is mostly hampered by the inclusion of constant masks when training for a small and fixed number of training steps as in our case (results in tabular form are presented in Table 14).

Model	Forecasting horizon (hours)										
	6	24	48	72	96	120	144	168	192	216	240
Circular Pad UNet (4 Blocks w/ Zenith angle, and 2 input steps)	0.9823	0.9531	0.9099	0.8601	0.8071	0.7553	0.7089	0.6690	0.6370	0.6107	0.5880
Circular Pad UNet (4 Blocks w/ Zenith angle, 2 input steps, and constant masks)	0.9810	0.9506	0.9079	0.8604	0.8106	0.7616	0.7172	0.6792	<b>0.6479</b>	<b>0.6216</b>	<b>0.5980</b>
Circular Pad UNet (5 Blocks w/ Zenith angle, and 2 input steps)	<b>0.9846</b>	<b>0.9597</b>	<b>0.9246</b>	<b>0.8831</b>	<b>0.8352</b>	<b>0.7822</b>	<b>0.7293</b>	<b>0.6806</b>	0.6381	0.6025	0.5727
Circular Pad UNet (5 Blocks w/ Zenith angle, 2 input steps, and constant masks)	0.9827	0.9559	0.9170	0.8703	0.8182	0.7649	0.7153	0.6711	0.6324	0.5993	0.5701

(a) Geometric ACC

Model	Forecasting horizon (hours)										
	6	24	48	72	96	120	144	168	192	216	240
Circular Pad UNet (4 Blocks w/ Zenith angle, and 2 input steps)	0.1869	0.3014	0.4141	0.5141	0.6049	0.6870	0.7608	0.8299	0.8968	0.9648	1.0346
Circular Pad UNet (4 Blocks w/ Zenith angle, 2 input steps, and constant masks)	0.1934	0.3086	0.4168	0.5114	0.5969	0.6740	0.7411	<b>0.7997</b>	<b>0.8522</b>	<b>0.9025</b>	<b>0.9549</b>
Circular Pad UNet (5 Blocks w/ Zenith angle, and 2 input steps)	<b>0.1740</b>	<b>0.2801</b>	<b>0.3802</b>	<b>0.4709</b>	<b>0.5584</b>	<b>0.6445</b>	<b>0.7259</b>	0.8007	0.8676	0.9261	0.9774
Circular Pad UNet (5 Blocks w/ Zenith angle, 2 input steps, and constant masks)	0.1840	0.2929	0.3979	0.4949	0.5875	0.6759	0.7599	0.8427	0.9273	1.0141	1.1044

(b) Geometric RMSE

Table 14: **Geometric ACC (a) and RMSE (b) with the addition of static constant masks including topography, soil-type, and land-sea mask following (Bi et al., 2022).** The table highlights an interesting trend where the performance is mostly hampered by the inclusion of constant masks when training for a small and fixed number of training steps as in our case (results in graphical form are presented in Fig. 15).

while having a negligible detrimental effect on the short-horizon forecast. In particular, Perlin noise (Perlin, 2002), being structured, outperforms unstructured additive Gaussian noise. This gain in performance, however, is very likely to impact the ability to generate prediction ensembles via input state perturbation as the model learns to be invariant to this additive noise.

Note that we only evaluate on a fixed noise level, and skip a detailed ablation over different noise levels. We consider a more thorough analysis regarding the impact of noise during model training, not only for deterministic forecasts but also when trying to generate prediction ensembles as the model is directly trained with noise as interesting directions to explore further.

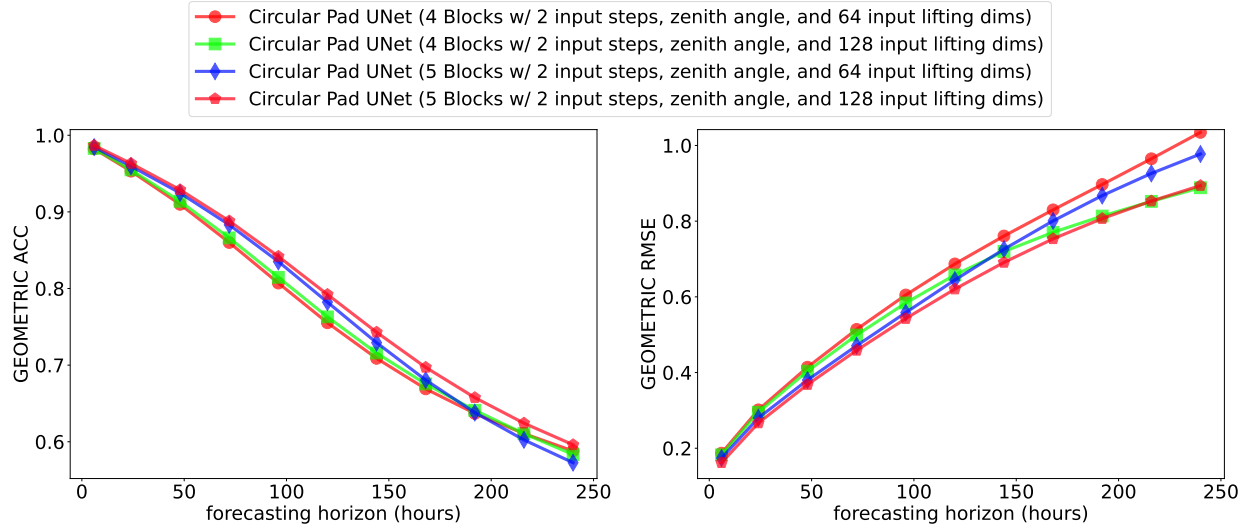


Figure 16: **Geometric ACC (left) and RMSE (right) with wider models i.e., larger hidden dimension.** We observe consistent gains with wider networks i.e., with an increased number of parameters for both 4-block and 5-block UNet variants (results in tabular form are presented in Table 15).

Model	Forecasting horizon (hours)										
	6	24	48	72	96	120	144	168	192	216	240
Circular Pad UNet (4 Blocks w/ 2 input steps, zenith angle, and 64 input lifting dims)	0.9823	0.9531	0.9099	0.8601	0.8071	0.7553	0.7089	0.6690	0.6370	0.6107	0.5880
Circular Pad UNet (4 Blocks w/ 2 input steps, zenith angle, and 128 input lifting dims)	0.9829	0.9548	0.9138	0.8660	0.8146	0.7630	0.7158	0.6754	0.6411	0.6106	0.5834
Circular Pad UNet (5 Blocks w/ 2 input steps, zenith angle, and 64 input lifting dims)	0.9846	0.9597	0.9246	0.8831	0.8352	0.7822	0.7293	0.6806	0.6381	0.6025	0.5727
Circular Pad UNet (5 Blocks w/ 2 input steps, zenith angle, and 128 input lifting dims)	<b>0.9867</b>	<b>0.9632</b>	<b>0.9288</b>	<b>0.8881</b>	<b>0.8419</b>	<b>0.7922</b>	<b>0.7430</b>	<b>0.6971</b>	<b>0.6576</b>	<b>0.6243</b>	<b>0.5961</b>

(a) Geometric ACC

Model	Forecasting horizon (hours)										
	6	24	48	72	96	120	144	168	192	216	240
Circular Pad UNet (4 Blocks w/ 2 input steps, zenith angle, and 64 input lifting dims)	0.1869	0.3014	0.4141	0.5141	0.6049	0.6870	0.7608	0.8299	0.8968	0.9648	1.0346
Circular Pad UNet (4 Blocks w/ 2 input steps, zenith angle, and 128 input lifting dims)	0.1826	0.2951	0.4037	0.4991	0.5838	0.6579	0.7198	0.7705	0.8135	<b>0.8523</b>	<b>0.8883</b>
Circular Pad UNet (5 Blocks w/ 2 input steps, zenith angle, and 64 input lifting dims)	0.1740	0.2801	0.3802	0.4709	0.5584	0.6445	0.7259	0.8007	0.8676	0.9261	0.9774
Circular Pad UNet (5 Blocks w/ 2 input steps, zenith angle, and 128 input lifting dims)	<b>0.1618</b>	<b>0.2667</b>	<b>0.3682</b>	<b>0.4586</b>	<b>0.5426</b>	<b>0.6205</b>	<b>0.6910</b>	<b>0.7533</b>	<b>0.8068</b>	0.8530	0.8940

(b) Geometric RMSE

Table 15: **Geometric ACC (a) and RMSE (b) with wider models i.e., larger hidden dimension.** We observe consistent gains with wider networks i.e., with an increased number of parameters for both 4-block and 5-block UNet variants (results in graphical form are presented in Fig. 16).

## 4.9 Impact of appending 3D coordinates

As a fixed-sized grid is not natural for weather forecasting due to the underlying spherical structure of the globe, and limits querying the model on any arbitrary grid point, resolution invariant models that use the query location coordinates as input to generate predictions have been a major focus (Pathak et al., 2022; Bonev et al., 2023; Lam et al., 2022).

This 3D coordinate information is useful for the model to understand the proximity in 3D space (specifically close to the poles due to oversampling when projecting to a fixed-sized lat-long grid). Latitude-weighted loss functions have been used to circumvent this issue partially due to this oversampling. In our architecture search, we also used several 3D methods that directly use this 3D coordinate information. This coordinate information can also potentially be useful for even image-based models as used in prior models such as CoordConv (Liu et al., 2018).

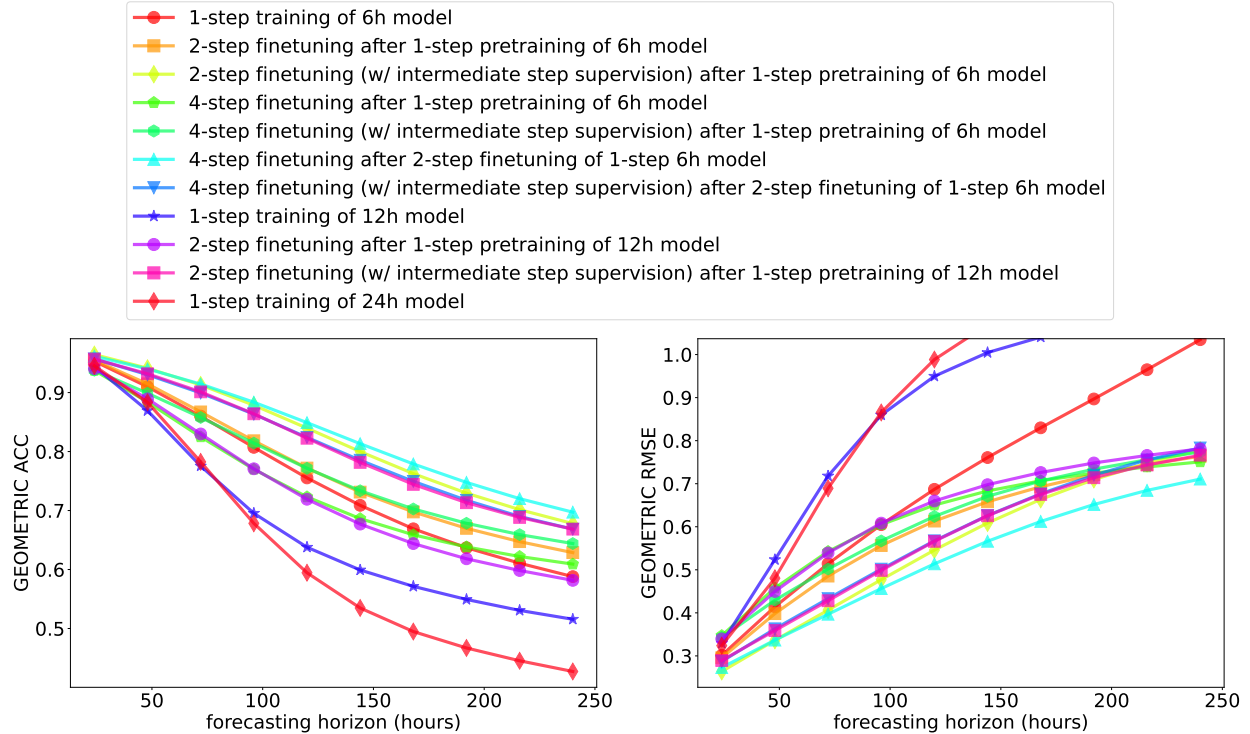


Figure 17: **Geometric ACC (left) and RMSE (right) with multi-step fine-tuning for 4-block UNet.** The figure highlights that training the model with the smallest stride considered i.e., 6h coupled with sequential fine-tuning provides the best performance, which has been the most common choice in the past (results in tabular form are presented in Table 16).

Therefore, we experiment with appending 3D coordinates converted from the lat-long grid as three additional input channels representing the x, y, and z coordinates on the sphere respectively. As this is input-independent, we add a single set of x, y, and z coordinates even for multi-step models.

The geometric ACC and RMSE with the inclusion of 3D location coordinates as additional static channels are presented in Table 11 (Fig. 12). The results highlight the positive impact of appending the 3D coordinates, specifically for the long-horizon prediction task. There is however a disparity between the two model sizes where 5-block UNet seems to be benefitting more from this auxiliary information. This highlights the fact that the utility of each of these approaches can change significantly given the exact model in question. This is a recurring theme for many of our subsequent results.

#### 4.10 Impact of loss functions

Most prior works experimented with different loss functions, such as Geometric MSE (Pathak et al., 2022; Bonev et al., 2023; Lam et al., 2022; Nguyen et al., 2023b) or geometric  $L_1$  (Chen et al., 2023). We attempt to evaluate the impact of different loss functions on the predictive performance of the resulting model, which includes regular MSE which is equivalent to  $L_2^2$  (the default loss function that we use to train all our models), geometric MSE,  $L_1$  loss, geometric  $L_1$ , Huber (smooth  $L_1$ ), and  $L_1$ - $L_2$  loss (with a weight of 0.05 assigned to  $L_1$  loss and 0.95 assigned to  $L_2^2$  loss). Note that we did not explore the impact of weighing the variables or the pressure levels differently as explored

Model	Forecasting horizon (hours)									
	24	48	72	96	120	144	168	192	216	240
1-step training of 6h model	0.9531	0.9099	0.8601	0.8071	0.7553	0.7089	0.6690	0.6370	0.6107	0.5880
2-step finetuning after 1-step pretraining of 6h model	0.9550	0.9148	0.8673	0.8183	0.7721	0.7313	0.6976	0.6698	0.6473	0.6286
2-step finetuning (w/ intermediate step supervision) after 1-step pretraining of 6h model	<b>0.9645</b>	<b>0.9413</b>	0.9129	0.8786	0.8397	0.8000	0.7626	0.7295	0.7015	0.6779
4-step finetuning after 1-step pretraining of 6h model	0.9376	0.8840	0.8249	0.7700	0.7232	0.6863	0.6589	0.6383	0.6221	0.6092
4-step finetuning (w/ intermediate step supervision) after 1-step pretraining of 6h model	0.9379	0.8989	0.8578	0.8143	0.7716	0.7336	0.7027	0.6784	0.6592	0.6440
4-step finetuning after 2-step finetuning of 1-step 6h model	0.9617	0.9402	<b>0.9144</b>	<b>0.8837</b>	<b>0.8491</b>	<b>0.8134</b>	<b>0.7790</b>	<b>0.7477</b>	<b>0.7202</b>	<b>0.6972</b>
4-step finetuning (w/ intermediate step supervision) after 2-step finetuning of 1-step 6h model	0.9572	0.9303	0.8993	0.8634	0.8241	0.7853	0.7495	0.7173	0.6900	0.6684
1-step training of 12h model	0.9444	0.8693	0.7755	0.6953	0.6378	0.5992	0.5714	0.5493	0.5307	0.5157
2-step finetuning after 1-step pretraining of 12h model	0.9405	0.8894	0.8298	0.7708	0.7191	0.6770	0.6440	0.6182	0.5983	0.5816
2-step finetuning (w/ intermediate step supervision) after 1-step pretraining of 12h model	0.9567	0.9319	0.9012	0.8640	0.8226	0.7816	0.7444	0.7133	0.6883	0.6685
1-step training of 24h model	0.9453	0.8835	0.7825	0.6783	0.5945	0.5348	0.4948	0.4670	0.4453	0.4272

(a) Geometric ACC

Model	Forecasting horizon (hours)									
	24	48	72	96	120	144	168	192	216	240
1-step training of 6h model	0.3014	0.4141	0.5141	0.6049	0.6870	0.7608	0.8299	0.8968	0.9648	1.0346
2-step finetuning after 1-step pretraining of 6h model	0.2956	0.3982	0.4854	0.5564	0.6131	0.6580	0.6929	0.7212	0.7442	0.7638
2-step finetuning (w/ intermediate step supervision) after 1-step pretraining of 6h model	<b>0.2638</b>	<b>0.3362</b>	0.4064	0.4771	0.5458	0.6087	0.6635	0.7097	0.7471	0.7781
4-step finetuning after 1-step pretraining of 6h model	0.3472	0.4577	0.5426	0.6048	0.6503	0.6831	0.7068	0.7247	0.7389	0.7507
4-step finetuning (w/ intermediate step supervision) after 1-step pretraining of 6h model	0.3428	0.4293	0.5018	0.5670	0.6240	0.6706	0.7063	0.7338	0.7556	0.7737
4-step finetuning after 2-step finetuning of 1-step 6h model	0.2729	0.3367	<b>0.3968</b>	<b>0.4564</b>	<b>0.5138</b>	<b>0.5662</b>	<b>0.6123</b>	<b>0.6517</b>	<b>0.6844</b>	<b>0.7107</b>
4-step finetuning (w/ intermediate step supervision) after 2-step finetuning of 1-step 6h model	0.2871	0.3629	0.4330	0.5015	0.5674	0.6260	0.6766	0.7198	0.7553	0.7830
1-step training of 12h model	0.3293	0.5236	0.7180	0.8595	0.9496	1.0046	1.0406	1.0674	1.0886	1.1062
2-step finetuning after 1-step pretraining of 12h model	0.3395	0.4497	0.5391	0.6084	0.6598	0.6977	0.7261	0.7482	0.7657	0.7810
2-step finetuning (w/ intermediate step supervision) after 1-step pretraining of 12h model	0.2894	0.3589	0.4281	0.4986	0.5662	0.6256	0.6751	0.7139	0.7435	0.7662
1-step training of 24h model	0.3238	0.4804	0.6893	0.8655	0.9884	1.0692	1.1233	1.1637	1.1973	1.2257

(b) Geometric RMSE

Table 16: **Geometric ACC (a) and RMSE (b) with multi-step fine-tuning for 4-block UNet**. The table highlights that training the model with the smallest stride considered i.e., 6h coupled with sequential fine-tuning provides the best performance, which has been the most common choice in the past (results in graphical form are presented in Fig. 17).

in some other works (Lam et al., 2022; Nguyen et al., 2023b).

#### 4.10.1 UNet (4 Blocks)

The geometric ACC and RMSE for different loss functions on the 4-block UNet model are presented in Table 12 (Fig. 13). The figure highlights the superiority of  $L_1$ - $L_2$  loss when considering short-horizon predictions. However, when considering long-horizon predictions, geometric  $L_1$  loss dominates. In general, we observe better performance with  $L_1$  variants in contrast to  $L_2$  variants potentially due to its capacity to ignore outliers, which is particularly helpful during long auto-regressive rollouts.

#### 4.10.2 UNet (5 Blocks)

The geometric ACC and RMSE for different loss functions on the 5-block UNet model are presented in Table 13 (Fig. 14). In contrast to the 4-block UNet,  $L_2^2$  (MSE) variants dominate for the short-horizon forecast, while variants of  $L_1$  loss dominate in the long-horizon prediction. Interestingly,  $L_1$ - $L_2$  loss diverges in this case, highlighting a potential optimization instability with  $L_1$  variants. As seen previously, this highlights that different models might be best suited to different loss functions and hence, require a model-specific evaluation.

### 4.11 Impact of constant masks

Constant masks are static masks that provide additional information to the model that might be useful for prediction. Following Bi et al. (2022), we consider three constant masks including topography, soil type, and land-sea mask. As these masks are static, we only append them once even during the auto-regressive rollout. Since all our input channels are standardized based on the dataset

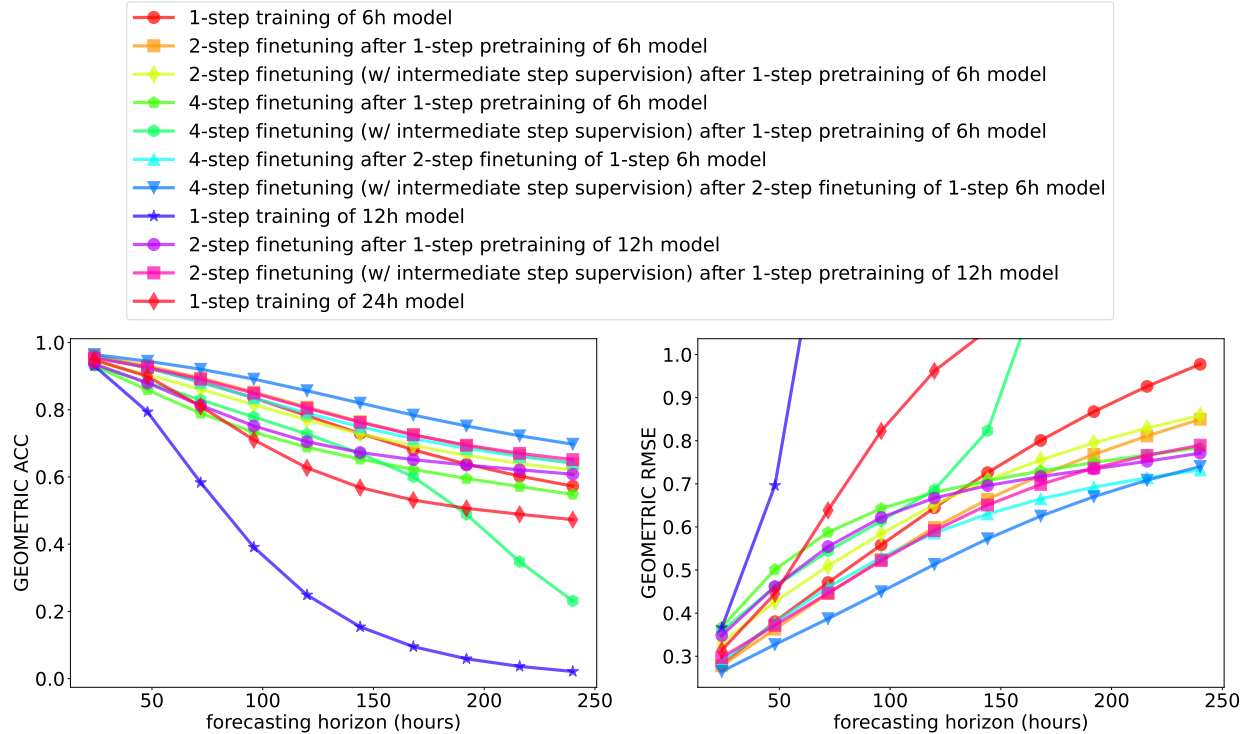


Figure 18: **Geometric ACC (left) and RMSE (right) with multi-step fine-tuning for 5-block UNet.** In contrast to 4-block UNet, we see that 5-block UNet benefits from intermediate step supervision for sequential fine-tuning (results in tabular form are presented in Table 17).

mean and standard deviation, we also standardize the constant masks based on the computed mean and standard deviation (note that this is again a constant as we are using static masks).

The geometric ACC and RMSE for constant mask comparison are presented in Table 14 (Fig. 15). We see a less pronounced effect in comparison to the zenith angle which always helps. We again see a model-specific impact where performance improves for the 4-block variant, but degrades for the 5-block variant of UNet. This is surprising as we would expect larger models to make better use of additional information. We speculate this to be an artifact of overfitting on these auxiliary static masks.

#### 4.12 Impact of wider models

The interplay between the depth and width of the model has been an interesting point of discussion in the past (Zagoruyko & Komodakis, 2016). In order to understand the gain in performance with model width, we experiment with increasing the starting embedding dimension of our model from 64. Note that we have an hourglass architecture, which results in doubling the number of channels after every spatial downsampling stage following the original UNet architecture (Ronneberger et al., 2015). In this case, we increase the number of channels from 64 which was the default for all our prior experiments to 128.

The geometric ACC and RMSE with an increased model width are presented in Table 15 (Fig. 16). The results highlight that increasing the hidden dimension of the model from 64 to 128 boosts model performance for both the 4-block and 5-block variants. However, the gain is more pronounced for the 5-block UNet, despite having an extremely large number of parameters in contrast to all other

Model	Forecasting horizon (hours)									
	24	48	72	96	120	144	168	192	216	240
1-step training of 6h model	0.9597	0.9246	0.8831	0.8352	0.7822	0.7293	0.6806	0.6381	0.6025	0.5727
2-step finetuning after 1-step pretraining of 6h model	0.9602	0.9310	0.8946	0.8526	0.8080	0.7646	0.7259	0.6924	0.6642	0.6407
2-step finetuning (w/ intermediate step supervision) after 1-step pretraining of 6h model	0.9436	0.9041	0.8610	0.8152	0.7693	0.7282	0.6936	0.6645	0.6400	0.6204
4-step finetuning after 1-step pretraining of 6h model	0.9308	0.8589	0.7896	0.7328	0.6883	0.6529	0.6226	0.5954	0.5713	0.5482
4-step finetuning (w/ intermediate step supervision) after 1-step pretraining of 6h model	0.9315	0.8811	0.8293	0.7785	0.7276	0.6701	0.6005	0.4889	0.3479	0.2312
4-step finetuning after 2-step finetuning of 1-step 6h model	0.9578	0.9241	0.8816	0.8354	0.7900	0.7492	0.7140	0.6850	0.6611	0.6412
4-step finetuning (w/ intermediate step supervision) after 2-step finetuning of 1-step 6h model	<b>0.9641</b>	<b>0.9443</b>	<b>0.9205</b>	<b>0.8911</b>	<b>0.8565</b>	<b>0.8197</b>	<b>0.7840</b>	<b>0.7516</b>	<b>0.7223</b>	<b>0.6975</b>
1-step training of 12h model	0.9307	0.7934	0.5831	0.3909	0.2488	0.1539	0.0951	0.0590	0.0364	0.0213
2-step finetuning after 1-step pretraining of 12h model	0.9363	0.8795	0.8131	0.7519	0.7048	0.6727	0.6515	0.6355	0.6213	0.6081
2-step finetuning (w/ intermediate step supervision) after 1-step pretraining of 12h model	0.9541	0.9261	0.8911	0.8493	0.8047	0.7623	0.7253	0.6946	0.6703	0.6515
1-step training of 24h model	0.9486	0.8991	0.8102	0.7105	0.6270	0.5683	0.5312	0.5066	0.4890	0.4730

(a) Geometric ACC

Model	Forecasting horizon (hours)									
	24	48	72	96	120	144	168	192	216	240
1-step training of 6h model	0.2801	0.3802	0.4709	0.5584	0.6445	0.7259	0.8007	0.8676	0.9261	0.9774
2-step finetuning after 1-step pretraining of 6h model	0.2778	0.3628	0.4454	0.5248	0.5986	0.6642	0.7201	0.7684	0.8110	0.8499
2-step finetuning (w/ intermediate step supervision) after 1-step pretraining of 6h model	0.3312	0.4266	0.5092	0.5844	0.6519	0.7086	0.7554	0.7952	0.8294	0.8587
4-step finetuning after 1-step pretraining of 6h model	0.3674	0.5013	0.5876	0.6428	0.6800	0.7074	0.7298	0.7496	0.7671	0.7838
4-step finetuning (w/ intermediate step supervision) after 1-step pretraining of 6h model	0.3579	0.4612	0.5441	0.6139	0.6862	0.8232	1.1680	1.9843	3.6692	6.7553
4-step finetuning after 2-step finetuning of 1-step 6h model	0.2875	0.3780	0.4598	0.5293	0.5858	0.6302	0.6650	0.6923	0.7141	<b>0.7321</b>
4-step finetuning (w/ intermediate step supervision) after 2-step finetuning of 1-step 6h model	<b>0.2646</b>	<b>0.3270</b>	<b>0.3871</b>	<b>0.4496</b>	<b>0.5129</b>	<b>0.5725</b>	<b>0.6253</b>	<b>0.6702</b>	<b>0.7086</b>	0.7401
1-step training of 12h model	0.3660	0.6962	1.4075	2.9213	5.5888	10.0250	17.3233	29.3110	49.0948	82.0989
2-step finetuning after 1-step pretraining of 12h model	0.3482	0.4617	0.5544	0.6220	0.6670	0.6961	0.7167	0.7346	0.7524	0.7712
2-step finetuning (w/ intermediate step supervision) after 1-step pretraining of 12h model	0.2969	0.3717	0.4465	0.5217	0.5913	0.6508	0.6988	0.7367	0.7660	0.7898
1-step training of 24h model	0.3142	0.4450	0.6386	0.8227	0.9621	1.0566	1.1184	1.1622	1.1962	1.2279

(b) Geometric RMSE

Table 17: **Geometric ACC (a) and RMSE (b) with multi-step fine-tuning for 5-block UNet.** In contrast to 4-block UNet, we see that 5-block UNet benefits from intermediate step supervision for sequential fine-tuning (results in graphical form are presented in Fig. 18).

models (i.e., 1.6 billion parameters as highlighted in Table 1). These findings are consistent with prior results in the computer vision literature, where they found a prominent effect of model width on performance (Zagoruyko & Komodakis, 2016).

### 4.13 Impact of multi-step fine-tuning

With the notable exception of Bi et al. (2022) where they used multiple models operating at different temporal resolutions, and Price et al. (2023) where a diffusion model was employed, all prior works rely on fine-tuning the base model for multi-step forecasting to enable the model to generate smooth long-horizon predictions (Pathak et al., 2022; Lam et al., 2022; Bonev et al., 2023). There are different choices involved in this case, where a complicated combination of temporal resolution, number of auto-regressive steps, and appropriate fine-tuning supervision are potential choices that one encounters.

We therefore attempt to understand the marginal impact of each of these complex design choices. We evaluate two variants of fine-tuning supervision in this case i.e., intermediate-step supervision and only last-step supervision. When using intermediate-step supervision, we use a discount factor of 0.9 for all the subsequent prediction steps starting with a weight of 1.0, in order to represent higher uncertainty as commonly used in reinforcement learning (Sutton, 2018). Even in the case of just supervising the model on the last step, the gradient is computed through the auto-regressive rollout trajectory. Note that the initial input is the same in all cases i.e., two input steps with a stride of 6h are concatenated regardless of the prediction temporal resolution of the model for consistency between results.

We only consider delta prediction formulation for our experiments. However, delta prediction might not be well-suited for larger stride models beyond the 6h horizon considered here. Therefore, there is a chance that these experiments greatly undermine the actual potential of larger stride models. We consider resolving this discrepancy and doing a more detailed analysis as an important

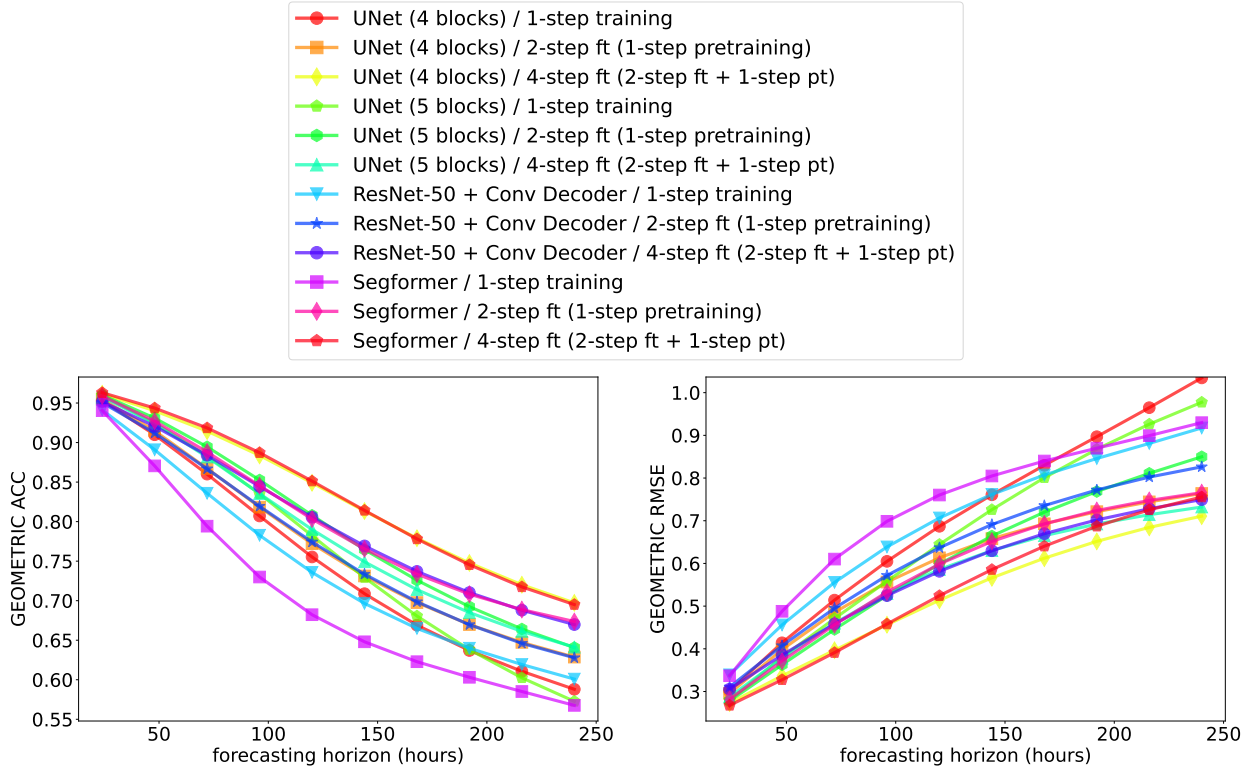


Figure 19: **Geometric ACC (left) and RMSE (right) with multi-step fine-tuning for comparing other promising models alongside UNet including ResNet-50 w/ convolutional decoder and Segformer.** All models are trained with the zenith angle. We see that multi-step fine-tuning improves performance significantly for all models evaluated (results in tabular form are presented in Table 18).

future direction.

#### 4.13.1 UNet (4 Blocks)

The results in terms of geometric ACC and RMSE for the 4 block UNet are presented Table 16 (Fig. 17). The results show a clear trend where fine-tuning the model on subsequently larger strides while only supervising the last step provides the best performance, surprisingly even better than supervising the intermediate steps of the model. This reaffirms the common practice of sequentially fine-tuning a small stride model (such as 6h) on increasingly larger prediction horizons (Pathak et al., 2022; Bonev et al., 2023; Lam et al., 2022).

Note that there is also a confounding variable in this case in the form of compute time. As each of our runs has a fixed budget of 10 epochs, sequential fine-tuning results in a direct increase in the allocated computational budget. The obtained conclusions might differ if each of these runs is trained till convergence.

#### 4.13.2 UNet (5 Blocks)

The results for the 5-block UNet are presented in Table 17 (Fig. 18). Similar to the 4-block UNet, we see that the model benefits from sequential fine-tuning. However, in contrast to the 4-block

Model	Forecasting horizon (hours)									
	24	48	72	96	120	144	168	192	216	240
UNet (4 blocks) / 1-step training	0.9531	0.9099	0.8601	0.8071	0.7553	0.7089	0.6690	0.6370	0.6107	0.5880
UNet (4 blocks) / 2-step ft (1-step pretraining)	0.9550	0.9148	0.8673	0.8183	0.7721	0.7313	0.6976	0.6698	0.6473	0.6286
UNet (4 blocks) / 4-step ft (2-step ft + 1-step pt)	0.9617	0.9402	0.9144	0.8837	0.8491	0.8134	<b>0.7790</b>	<b>0.7477</b>	<b>0.7202</b>	<b>0.6972</b>
UNet (5 blocks) / 1-step training	0.9597	0.9246	0.8831	0.8352	0.7822	0.7293	0.6806	0.6381	0.6025	0.5727
UNet (5 blocks) / 2-step ft (1-step pretraining)	0.9602	0.9310	0.8946	0.8526	0.8080	0.7646	0.7259	0.6924	0.6642	0.6407
UNet (5 blocks) / 4-step ft (2-step ft + 1-step pt)	0.9578	0.9241	0.8816	0.8354	0.7900	0.7492	0.7140	0.6850	0.6611	0.6412
ResNet-50 + Conv Decoder / 1-step training	0.9413	0.8909	0.8359	0.7828	0.7358	0.6965	0.6649	0.6399	0.6193	0.6008
ResNet-50 + Conv Decoder / 2-step ft (1-step pretraining)	0.9505	0.9121	0.8668	0.8194	0.7743	0.7335	0.6986	0.6697	0.6461	0.6278
ResNet-50 + Conv Decoder / 4-step ft (2-step ft + 1-step pt)	0.9518	0.9206	0.8839	0.8445	0.8056	0.7693	0.7371	0.7103	0.6880	0.6698
Segformer / 1-step training	0.9404	0.8705	0.7942	0.7299	0.6823	0.6480	0.6228	0.6031	0.5851	0.5676
Segformer / 2-step ft (1-step pretraining)	0.9589	0.9271	0.8881	0.8454	0.8032	0.7654	0.7336	0.7083	0.6887	0.6737
Segformer / 4-step ft (2-step ft + 1-step pt)	<b>0.9631</b>	<b>0.9436</b>	<b>0.9185</b>	<b>0.8872</b>	<b>0.8512</b>	<b>0.8142</b>	0.7781	0.7455	0.7174	0.6950

(a) Geometric ACC

Model	Forecasting horizon (hours)									
	24	48	72	96	120	144	168	192	216	240
UNet (4 blocks) / 1-step training	0.3014	0.4141	0.5141	0.6049	0.6870	0.7608	0.8299	0.8968	0.9648	1.0346
UNet (4 blocks) / 2-step ft (1-step pretraining)	0.2956	0.3982	0.4854	0.5564	0.6131	0.6580	0.6929	0.7212	0.7442	0.7638
UNet (4 blocks) / 4-step ft (2-step ft + 1-step pt)	0.2729	0.3367	0.3968	<b>0.4564</b>	<b>0.5138</b>	<b>0.5662</b>	<b>0.6123</b>	<b>0.6517</b>	<b>0.6844</b>	<b>0.7107</b>
UNet (5 blocks) / 1-step training	0.2801	0.3802	0.4709	0.5584	0.6445	0.7259	0.8007	0.8676	0.9261	0.9774
UNet (5 blocks) / 2-step ft (1-step pretraining)	0.2778	0.3628	0.4454	0.5248	0.5986	0.6642	0.7201	0.7684	0.8110	0.8499
UNet (5 blocks) / 4-step ft (2-step ft + 1-step pt)	0.2875	0.3780	0.4598	0.5293	0.5858	0.6302	0.6650	0.6923	0.7141	0.7321
ResNet-50 + Conv Decoder / 1-step training	0.3391	0.4559	0.5556	0.6387	0.7065	0.7616	0.8071	0.8457	0.8811	0.9173
ResNet-50 + Conv Decoder / 2-step ft (1-step pretraining)	0.3107	0.4073	0.4951	0.5718	0.6368	0.6911	0.7355	0.7721	0.8022	0.8262
ResNet-50 + Conv Decoder / 4-step ft (2-step ft + 1-step pt)	0.3055	0.3853	0.4586	0.5245	0.5815	0.6297	0.6697	0.7019	0.7281	0.7495
Segformer / 1-step training	0.3370	0.4879	0.6102	0.6987	0.7602	0.8048	0.8399	0.8699	0.8993	0.9297
Segformer / 2-step ft (1-step pretraining)	0.2818	0.3712	0.4562	0.5330	0.5987	0.6515	0.6926	0.7240	0.7476	0.7658
Segformer / 4-step ft (2-step ft + 1-step pt)	<b>0.2675</b>	<b>0.3276</b>	<b>0.3911</b>	0.4580	0.5245	0.5856	0.6404	0.6871	0.7255	0.7555

(b) Geometric RMSE

Table 18: **Geometric ACC with multi-step fine-tuning for comparing other promising models alongside UNet including ResNet-50 w/ convolutional decoder and Segformer.** All models are trained with the zenith angle. We see that multi-step fine-tuning improves performance significantly for all models evaluated (results in graphical form are presented in Fig. 19).

model, the model benefits from intermediate-step supervision. This again highlights that the exact fine-tuning recipe to be used might differ based on the model in question.

#### 4.14 Comparing best models with multi-step fine-tuning

We initially picked one model i.e., UNet (Ronneberger et al., 2015) out of multiple other promising models including ResNet-50 with fully-convolutional decoder (Long et al., 2015), Segformer (Xie et al., 2021), and SETR (Zheng et al., 2021) from our initial architecture search in Section 4.2. To understand the full potential of these models, we evaluate them again with the inclusion of the uncovered important design choices i.e., using 2-input steps, zenith angle, and multi-step fine-tuning.

We compare the performance between these models in Table 18 (Fig. 19). We adopt the sequential fine-tuning scheme in this case, supervising only the last step. Since this is ideal for the 4-block UNet, but not the 5-block variant, we see that the performance of our 4-block model outcompetes the 5-block variant in this case. Furthermore, Segformer achieves performance comparable to our 4-block UNet, while ResNet-50 with convolutional decoder follows the performance of our 5-block UNet. Note that Segformer without fine-tuning is the worst model in the plot with a large margin, again highlighting the importance of multi-step fine-tuning for these models to work well.

Note that we excluded SETR for comparison here despite it being a competitive model due to memory constraints. We assume the performance for SETR would be similar to that of Segformer as both are based on the transformer architecture (Vaswani et al., 2017).

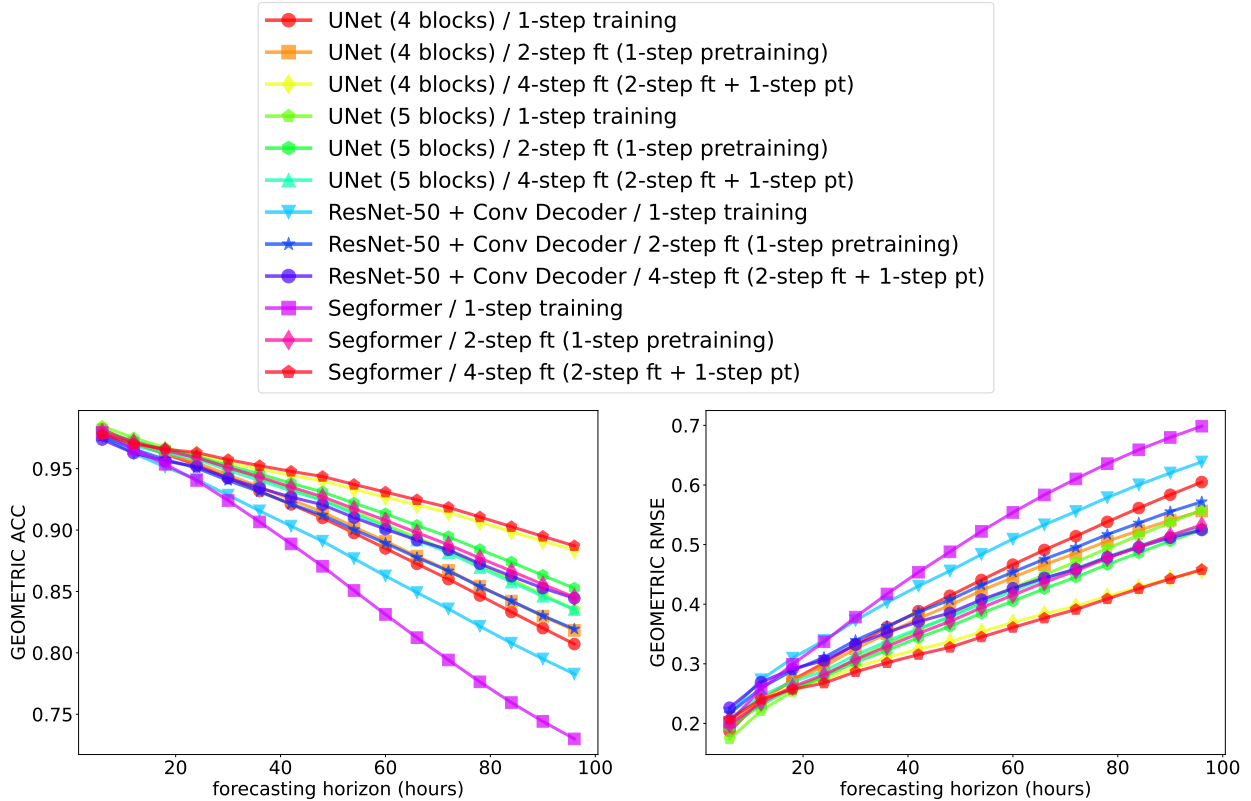


Figure 20: **Geometric ACC (left) and RMSE (right) when focusing on short-horizon forecast with multi-step fine-tuning for comparing other promising models alongside UNet including ResNet-50 w/ convolutional decoder and Segformer.** All models are trained with the zenith angle. We see that multi-step fine-tuning improves performance significantly for all models evaluated (see Fig. 19 for results over longer horizon – results in tabular form are presented in Table 19).

#### 4.14.1 Focusing on short-horizon forecasting

As our previous results were plotted with a larger stride of a day, we now focus on having a deeper look at the short-term forecast by plotting the results at the lowest granularity i.e., 6h prediction. The results are presented in Table 19 (Fig. 20) respectively. These results are fully consistent with previous results due to smoothness where we see best performance from Segformer and 4-block UNet variants.

### 4.15 Impact of training on a larger dataset

All our experiments prior focused on training the model on a 6h dataset variant sampled at 0000, 0600, 1200, and 1800 UTC (Pathak et al., 2022; Lam et al., 2022; Bonev et al., 2023). However, ERA5 naturally provides an hourly snapshot. Therefore, we further evaluate the impact of training the model on this hourly snapshot while retaining the 6h prediction horizon, resulting in 6x more training examples. Training the model on this hourly dataset for 10 epochs is equivalent to training the model on the 6h dataset for 60 epochs in terms of the number of training steps. Therefore, we add the 60 epochs baseline on the 6h dataset as a comparison which matches the computational budget for training on the 1h dataset for 10 epochs. For a fair comparison, we evaluate our models

Model	Forecasting horizon (hours)															
	6	12	18	24	30	36	42	48	54	60	66	72	78	84	90	96
UNet (4 blocks) / 1-step training	0.9823	0.9709	0.9619	0.9531	0.9426	0.9318	0.9209	0.9099	0.8976	0.8851	0.8725	0.8601	0.8467	0.8333	0.8201	0.8071
UNet (4 blocks) / 2-step ft (1-step pretraining)	0.9795	0.9705	0.9621	0.9550	0.9449	0.9353	0.9248	0.9148	0.9026	0.8910	0.8788	0.8673	0.8544	0.8422	0.8298	0.8183
UNet (4 blocks) / 4-step ft (2-step ft + 1-step pt)	0.9781	0.9699	0.9650	0.9617	0.9552	0.9497	0.9446	0.9402	0.9333	0.9268	0.9204	0.9144	0.9065	0.8987	0.8910	0.8837
UNet (5 blocks) / 1-step training	<b>0.9846</b>	<b>0.9751</b>	<b>0.9670</b>	0.9597	0.9511	0.9424	0.9336	0.9246	0.9147	0.9043	0.8938	0.8831	0.8715	0.8596	0.8475	0.8352
UNet (5 blocks) / 2-step ft (1-step pretraining)	0.9805	0.9726	0.9655	0.9602	0.9525	0.9457	0.9381	0.9310	0.9219	0.9132	0.9038	0.8946	0.8841	0.8739	0.8631	0.8526
UNet (5 blocks) / 4-step ft (2-step ft + 1-step pt)	0.9776	0.9687	0.9625	0.9578	0.9487	0.9404	0.9320	0.9241	0.9131	0.9025	0.8918	0.8816	0.8695	0.8576	0.8461	0.8354
ResNet-50 + Conv Decoder / 1-step training	0.9763	0.9624	0.9515	0.9413	0.9285	0.9157	0.9032	0.8909	0.8767	0.8627	0.8491	0.8359	0.8217	0.8079	0.7951	0.7828
ResNet-50 + Conv Decoder / 2-step ft (1-step pretraining)	0.9762	0.9660	0.9575	0.9505	0.9404	0.9312	0.9213	0.9121	0.9003	0.8893	0.8776	0.8668	0.8540	0.8423	0.8302	0.8194
ResNet-50 + Conv Decoder / 4-step ft (2-step ft + 1-step pt)	0.9737	0.9627	0.9562	0.9518	0.9423	0.9342	0.9268	0.9206	0.9101	0.9008	0.8918	0.8839	0.8726	0.8624	0.8527	0.8445
Segformer / 1-step training	0.9794	0.9660	0.9536	0.9404	0.9241	0.9066	0.8887	0.8705	0.8508	0.8313	0.8124	0.7942	0.7764	0.7595	0.7442	0.7299
Segformer / 2-step ft (1-step pretraining)	0.9801	0.9719	0.9648	0.9589	0.9508	0.9433	0.9350	0.9271	0.9174	0.9079	0.8979	0.8881	0.8772	0.8666	0.8558	0.8454
Segformer / 4-step ft (2-step ft + 1-step pt)	0.9779	0.9702	0.9659	<b>0.9631</b>	<b>0.9573</b>	<b>0.9524</b>	<b>0.9478</b>	<b>0.9436</b>	<b>0.9371</b>	<b>0.9309</b>	<b>0.9246</b>	<b>0.9185</b>	<b>0.9107</b>	<b>0.9028</b>	<b>0.8949</b>	<b>0.8872</b>

(a) Geometric ACC

Model	Forecasting horizon (hours)															
	6	12	18	24	30	36	42	48	54	60	66	72	78	84	90	96
UNet (4 blocks) / 1-step training	0.1869	0.2388	0.2728	0.3014	0.3325	0.3613	0.3884	0.4141	0.4406	0.4663	0.4910	0.5141	0.5381	0.5612	0.5836	0.6049
UNet (4 blocks) / 2-step ft (1-step pretraining)	0.1988	0.2402	0.2715	0.2956	0.3254	0.3507	0.3759	0.3982	0.4229	0.4448	0.4663	0.4854	0.5056	0.5236	0.5410	0.5564
UNet (4 blocks) / 4-step ft (2-step ft + 1-step pt)	0.2062	0.2416	0.2607	0.2729	0.2938	0.3102	0.3246	0.3367	0.3538	0.3693	0.3838	0.3968	0.4132	0.4285	0.4431	<b>0.4564</b>
UNet (5 blocks) / 1-step training	<b>0.1740</b>	<b>0.2211</b>	<b>0.2536</b>	0.2801	0.3078	0.3333	0.3573	0.3802	0.4038	0.4269	0.4494	0.4709	0.4935	0.5155	0.5372	0.5248
UNet (5 blocks) / 2-step ft (1-step pretraining)	0.1939	0.2311	0.2586	0.2778	0.3024	0.3227	0.3439	0.3628	0.3849	0.4051	0.4260	0.4454	0.4666	0.4862	0.5061	0.5248
UNet (5 blocks) / 4-step ft (2-step ft + 1-step pt)	0.2076	0.2463	0.2701	0.2875	0.3147	0.3378	0.3591	0.3780	0.4012	0.4224	0.4423	0.4598	0.4796	0.4978	0.5146	0.5293
ResNet-50 + Conv Decoder / 1-step training	0.2172	0.2733	0.3095	0.3391	0.3727	0.4029	0.4304	0.4559	0.4834	0.5092	0.5332	0.5556	0.5787	0.6003	0.6202	0.6387
ResNet-50 + Conv Decoder / 2-step ft (1-step pretraining)	0.2165	0.2594	0.2889	0.3107	0.3393	0.3629	0.3866	0.4073	0.4319	0.4537	0.4756	0.4951	0.5169	0.5361	0.5552	0.5718
ResNet-50 + Conv Decoder / 4-step ft (2-step ft + 1-step pt)	0.2263	0.2692	0.2915	0.3055	0.3321	0.3527	0.3707	0.3853	0.4077	0.4266	0.4441	0.4586	0.4786	0.4957	0.5115	0.5245
Segformer / 1-step training	0.2020	0.2576	0.2992	0.3370	0.3783	0.4172	0.4536	0.4879	0.5222	0.5539	0.5833	0.6102	0.6358	0.6590	0.6797	0.6987
Segformer / 2-step ft (1-step pretraining)	0.1977	0.2348	0.2614	0.2818	0.3070	0.3288	0.3509	0.3712	0.3940	0.4152	0.4365	0.4562	0.4771	0.4965	0.5155	0.5330
Segformer / 4-step ft (2-step ft + 1-step pt)	0.2074	0.2406	0.2571	<b>0.2675</b>	<b>0.2865</b>	<b>0.3017</b>	<b>0.3155</b>	<b>0.3276</b>	<b>0.3449</b>	<b>0.3609</b>	<b>0.3765</b>	<b>0.3911</b>	<b>0.4089</b>	<b>0.4259</b>	<b>0.4425</b>	0.4580

(b) Geometric RMSE

Table 19: **Geometric ACC (a) and RMSE (b) when focusing on short-horizon forecast with multi-step fine-tuning for comparing other promising models alongside UNet including ResNet-50 w/ convolutional decoder and Segformer.** All models are trained with the zenith angle. We see that multi-step fine-tuning improves performance significantly for all models evaluated (results in graphical form are presented in Fig. 20).

on the same 6h out-of-sample set that we used for all our prior evaluations.

The results are presented in Table 20 (Fig. 21). Similar to some of our prior results, we observe differences between the 4-block and 5-block UNet variants in this case, where training on the smaller dataset for longer degrades performance. This can be attributed to the overfitting of the model on the training set. However, the performance improves when training on the larger dataset. Our 5-block UNet on the other hand achieves similar performance in both cases i.e., training for longer on the smaller dataset and training for shorter on the larger dataset.

As the performance is always better or on par with the performance achieved by training on the smaller dataset, this indicates that using more data should be preferred wherever possible instead of training for longer on the smaller dataset.

## 5 Conclusion

In this paper, we attempt to analyze the role of different design choices on the performance of the resulting weather forecasting system. Our analysis shows that (unsurprisingly) architectures have a very strong impact on performance, where fixed-grid models outperform their grid-invariant counterparts. We further show that it is better to perform residual prediction when considering short-horizon prediction such as 6h considered in this work, regardless of the choice of architecture. In addition, we analyzed the impact of pretraining objectives, the use of image-based pretrained models, the number of past input steps, loss functions for training, as well as multi-step fine-tuning aside from several other more trivial explorations. We hope that these results would be useful in understanding the marginal contribution of different design choices for the training of weather forecasting systems, and hence, enable the development of better systems in the future.

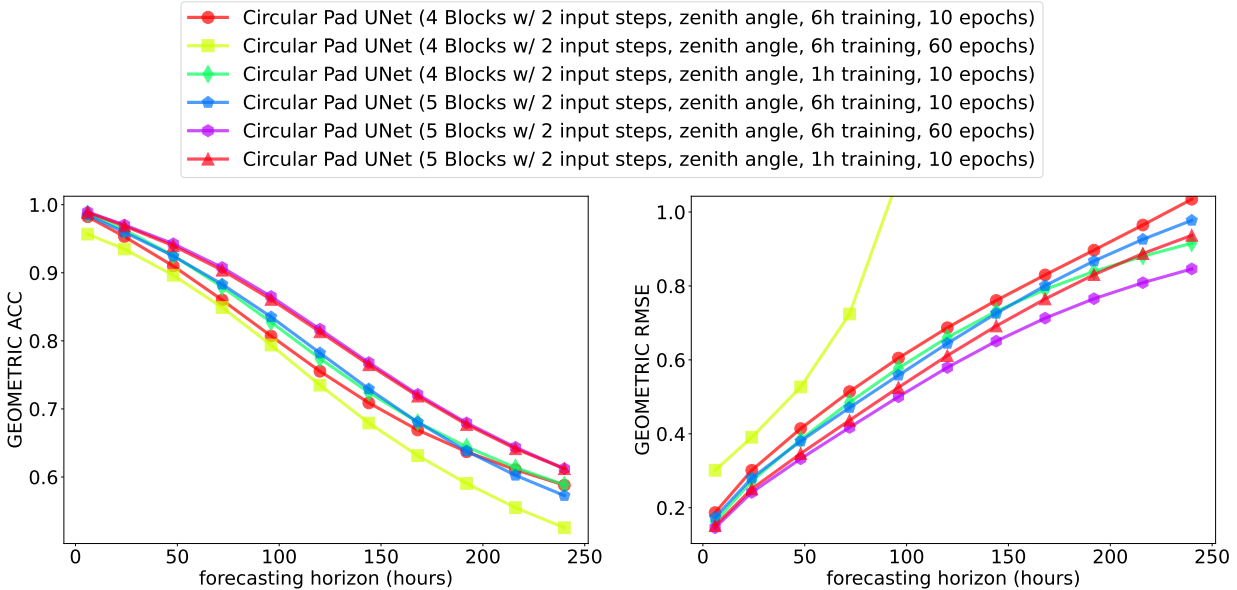


Figure 21: **Geometric ACC (left) and RMSE (right) when training on a larger dataset.** The figure highlights that training on the smaller dataset for longer is detrimental to the performance of the 4-block UNet which shows signs of overfitting, but training on the larger dataset improves performance. On the other hand, 5-block UNet effectively achieves similar performance in both cases, highlighting that different models might benefit differently from increased training data (results in tabular form are presented in Table 20).

## 6 Acknowledgements

The authors would like to thank Pedram Hassanzadeh for his valuable suggestions, and Thorsten Kurth for help with the datasets.

## References

- Md Ashiqur Rahman, Zachary E Ross, and Kamyar Azizzadenesheli. U-no: U-shaped neural operators. *arXiv e-prints*, pp. arXiv-2204, 2022.
- Samy Bengio, Oriol Vinyals, Navdeep Jaitly, and Noam Shazeer. Scheduled sampling for sequence prediction with recurrent neural networks. *Advances in neural information processing systems*, 28, 2015.
- Yoshua Bengio, Li Yao, Guillaume Alain, and Pascal Vincent. Generalized denoising auto-encoders as generative models. *Advances in neural information processing systems*, 26, 2013.
- Kaifeng Bi, Lingxi Xie, Hengheng Zhang, Xin Chen, Xiaotao Gu, and Qi Tian. Pangu-weather: A 3d high-resolution model for fast and accurate global weather forecast. *arXiv preprint arXiv:2211.02556*, 2022.
- Cristian Bodnar, Wessel P Bruinsma, Ana Lucic, Megan Stanley, Johannes Brandstetter, Patrick Garvan, Maik Riechert, Jonathan Weyn, Haiyu Dong, Anna Vaughan, et al. Aurora: A foundation model of the atmosphere. *arXiv preprint arXiv:2405.13063*, 2024.

Model	Forecasting horizon (hours)										
	6	24	48	72	96	120	144	168	192	216	240
Circular Pad UNet (4 Blocks w/ 2 input steps, zenith angle, 6h training, 10 epochs)	0.9823	0.9531	0.9099	0.8601	0.8071	0.7553	0.7089	0.6690	0.6370	0.6107	0.5880
Circular Pad UNet (4 Blocks w/ 2 input steps, zenith angle, 6h training, 60 epochs)	0.9568	0.9349	0.8964	0.8490	0.7939	0.7349	0.6793	0.6315	0.5905	0.5550	0.5255
Circular Pad UNet (4 Blocks w/ 2 input steps, zenith angle, 1h training, 10 epochs)	0.9869	0.9630	0.9252	0.8791	0.8275	0.7740	0.7241	0.6805	0.6443	0.6138	0.5885
Circular Pad UNet (5 Blocks w/ 2 input steps, zenith angle, 6h training, 10 epochs)	0.9846	0.9597	0.9246	0.8831	0.8352	0.7822	0.7293	0.6806	0.6381	0.6025	0.5727
Circular Pad UNet (5 Blocks w/ 2 input steps, zenith angle, 6h training, 60 epochs)	<b>0.9892</b>	<b>0.9702</b>	<b>0.9426</b>	<b>0.9077</b>	<b>0.8651</b>	<b>0.8170</b>	<b>0.7681</b>	<b>0.7214</b>	<b>0.6795</b>	<b>0.6435</b>	<b>0.6123</b>
Circular Pad UNet (5 Blocks w/ 2 input steps, zenith angle, 1h training, 10 epochs)	0.9887	0.9687	0.9397	0.9037	0.8609	0.8133	0.7649	0.7188	0.6771	0.6415	0.6122

(a) Geometric ACC

Model	Forecasting horizon (hours)										
	6	24	48	72	96	120	144	168	192	216	240
Circular Pad UNet (4 Blocks w/ 2 input steps, zenith angle, 6h training, 10 epochs)	0.1869	0.3014	0.4141	0.5141	0.6049	0.6870	0.7608	0.8299	0.8968	0.9648	1.0346
Circular Pad UNet (4 Blocks w/ 2 input steps, zenith angle, 6h training, 60 epochs)	0.3013	0.3906	0.5267	0.7242	1.0929	2.0225	4.5709	11.3957	27.4762	62.6718	142.4410
Circular Pad UNet (4 Blocks w/ 2 input steps, zenith angle, 1h training, 10 epochs)	0.1622	0.2722	0.3842	0.4853	0.5776	0.6606	0.7314	0.7905	0.8392	0.8803	0.9156
Circular Pad UNet (5 Blocks w/ 2 input steps, zenith angle, 6h training, 10 epochs)	0.1740	0.2801	0.3802	0.4709	0.5584	0.6445	0.7259	0.8007	0.8676	0.9261	0.9774
Circular Pad UNet (5 Blocks w/ 2 input steps, zenith angle, 6h training, 60 epochs)	<b>0.1459</b>	<b>0.2416</b>	<b>0.3325</b>	<b>0.4171</b>	<b>0.5002</b>	<b>0.5794</b>	<b>0.6505</b>	<b>0.7128</b>	<b>0.7655</b>	<b>0.8088</b>	<b>0.8460</b>
Circular Pad UNet (5 Blocks w/ 2 input steps, zenith angle, 1h training, 10 epochs)	0.1516	0.2509	0.3466	0.4365	0.5254	0.6115	0.6917	0.7648	0.8305	0.8876	0.9369

(b) Geometric RMSE

Table 20: **Geometric ACC (a) and RMSE (b) when training on a larger dataset.** The table highlights that training on the smaller dataset for longer is detrimental to the performance of the 4-block UNet which shows signs of overfitting, but training on the larger dataset improves performance. On the other hand, 5-block UNet effectively achieves similar performance in both cases, highlighting that different models might benefit differently from increased training data (results in graphical form are presented in Fig. 21).

Rishi Bommasani, Drew A Hudson, Ehsan Adeli, Russ Altman, Simran Arora, Sydney von Arx, Michael S Bernstein, Jeannette Bohg, Antoine Bosselut, Emma Brunskill, et al. On the opportunities and risks of foundation models. *arXiv preprint arXiv:2108.07258*, 2021.

Boris Bonev, Thorsten Kurth, Christian Hundt, Jaideep Pathak, Maximilian Baust, Karthik Kashinath, and Anima Anandkumar. Spherical fourier neural operators: Learning stable dynamics on the sphere. *arXiv preprint arXiv:2306.03838*, 2023.

Emmanuel Asiedu Brempong, Simon Kornblith, Ting Chen, Niki Parmar, Matthias Minderer, and Mohammad Norouzi. Denoising pretraining for semantic segmentation. In *Proceedings of the IEEE/CVF conference on computer vision and pattern recognition*, pp. 4175–4186, 2022.

Han Cai, Junyan Li, Muyan Hu, Chuang Gan, and Song Han. Efficientvit: Multi-scale linear attention for high-resolution dense prediction. *arXiv preprint arXiv:2205.14756*, 2022.

Lei Chen, Xiaohui Zhong, Feng Zhang, Yuan Cheng, Yinghui Xu, Yuan Qi, and Hao Li. Fuxi: A cascade machine learning forecasting system for 15-day global weather forecast. *arXiv preprint arXiv:2306.12873*, 2023.

Mark Chen, Alec Radford, Rewon Child, Jeffrey Wu, Heewoo Jun, David Luan, and Ilya Sutskever. Generative pretraining from pixels. In *International conference on machine learning*, pp. 1691–1703. PMLR, 2020.

Ricky TQ Chen, Yulia Rubanova, Jesse Bettencourt, and David K Duvenaud. Neural ordinary differential equations. *Advances in neural information processing systems*, 31, 2018.

Minjong Cheon, Yo-Hwan Choi, Seon-Yu Kang, Yumi Choi, Jeong-Gil Lee, and Daehyun Kang. Karina: An efficient deep learning model for global weather forecast. *arXiv preprint arXiv:2403.10555*, 2024.

- MMSegmentation Contributors. MMSegmentation: Openmmlab semantic segmentation toolbox and benchmark. <https://github.com/open-mmlab/msegmentation>, 2020.
- Alexey Dosovitskiy, Lucas Beyer, Alexander Kolesnikov, Dirk Weissenborn, Xiaohua Zhai, Thomas Unterthiner, Mostafa Dehghani, Matthias Minderer, Georg Heigold, Sylvain Gelly, et al. An image is worth 16x16 words: Transformers for image recognition at scale. *arXiv preprint arXiv:2010.11929*, 2020.
- Alaaeldin El-Nouby, Michal Klein, Shuangfei Zhai, Miguel Angel Bautista, Alexander Toshev, Vaishaal Shankar, Joshua M Susskind, and Armand Joulin. Scalable pre-training of large autoregressive image models. *arXiv preprint arXiv:2401.08541*, 2024.
- Dumitru Erhan, Pierre-Antoine Manzagol, Yoshua Bengio, Samy Bengio, and Pascal Vincent. The difficulty of training deep architectures and the effect of unsupervised pre-training. In *Artificial intelligence and statistics*, pp. 153–160. PMLR, 2009.
- Justin Gilmer, Samuel S Schoenholz, Patrick F Riley, Oriol Vinyals, and George E Dahl. Neural message passing for quantum chemistry. In *International conference on machine learning*, pp. 1263–1272. PMLR, 2017.
- Andre Graubner, Kamyar Kamyar Azizzadenesheli, Jaideep Pathak, Morteza Mardani, Mike Pritchard, Karthik Kashinath, and Anima Anandkumar. Calibration of large neural weather models. In *NeurIPS 2022 Workshop on Tackling Climate Change with Machine Learning*, 2022.
- John Guibas, Morteza Mardani, Zongyi Li, Andrew Tao, Anima Anandkumar, and Bryan Catanzaro. Adaptive fourier neural operators: Efficient token mixers for transformers. *arXiv preprint arXiv:2111.13587*, 2021.
- Kaiming He, Xiangyu Zhang, Shaoqing Ren, and Jian Sun. Deep residual learning for image recognition. In *Proceedings of the IEEE conference on computer vision and pattern recognition*, pp. 770–778, 2016.
- Kaiming He, Xinlei Chen, Saining Xie, Yanghao Li, Piotr Dollár, and Ross Girshick. Masked autoencoders are scalable vision learners. In *Proceedings of the IEEE/CVF conference on computer vision and pattern recognition*, pp. 16000–16009, 2022.
- Hans Hersbach, Bill Bell, Paul Berrisford, Shoji Hirahara, András Horányi, Joaquín Muñoz-Sabater, Julien Nicolas, Carole Peubey, Raluca Radu, Dinand Schepers, et al. The era5 global reanalysis. *Quarterly Journal of the Royal Meteorological Society*, 146(730):1999–2049, 2020.
- Langwen Huang, Lukas Gianinazzi, Yuejiang Yu, Peter D Dueben, and Torsten Hoeffler. Diffda: a diffusion model for weather-scale data assimilation. *arXiv preprint arXiv:2401.05932*, 2024.
- Peter J Huber. Robust estimation of a location parameter. In *Breakthroughs in statistics: Methodology and distribution*, pp. 492–518. Springer, 1992.
- Dmitrii Kochkov, Janni Yuval, Ian Langmore, Peter Norgaard, Jamie Smith, Griffin Mooers, James Lottes, Stephan Rasp, Peter Düben, Milan Klöwer, et al. Neural general circulation models. *arXiv preprint arXiv:2311.07222*, 2023.
- Alexander Kolesnikov, Lucas Beyer, Xiaohua Zhai, Joan Puigcerver, Jessica Yung, Sylvain Gelly, and Neil Houlsby. Big transfer (bit): General visual representation learning. In *Computer Vision—ECCV 2020: 16th European Conference, Glasgow, UK, August 23–28, 2020, Proceedings, Part V 16*, pp. 491–507. Springer, 2020.

- Remi Lam, Alvaro Sanchez-Gonzalez, Matthew Willson, Peter Wirnsberger, Meire Fortunato, Ferran Alet, Suman Ravuri, Timo Ewalds, Zach Eaton-Rosen, Weihua Hu, et al. Graphcast: Learning skillful medium-range global weather forecasting. *arXiv preprint arXiv:2212.12794*, 2022.
- Pablo Rozas Larraondo, Luigi J Renzullo, Inaki Inza, and Jose A Lozano. A data-driven approach to precipitation parameterizations using convolutional encoder-decoder neural networks. *arXiv preprint arXiv:1903.10274*, 2019.
- Yann LeCun, Bernhard Boser, John Denker, Donnie Henderson, Richard Howard, Wayne Hubbard, and Lawrence Jackel. Handwritten digit recognition with a back-propagation network. *Advances in neural information processing systems*, 2, 1989.
- Lizao Li, Robert Carver, Ignacio Lopez-Gomez, Fei Sha, and John Anderson. Generative emulation of weather forecast ensembles with diffusion models. *Science Advances*, 10(13):eadk4489, 2024a.
- Zongyi Li, Nikola Kovachki, Kamyar Azizzadenesheli, Burigede Liu, Kaushik Bhattacharya, Andrew Stuart, and Anima Anandkumar. Fourier neural operator for parametric partial differential equations. *arXiv preprint arXiv:2010.08895*, 2020a.
- Zongyi Li, Nikola Kovachki, Kamyar Azizzadenesheli, Burigede Liu, Kaushik Bhattacharya, Andrew Stuart, and Anima Anandkumar. Neural operator: Graph kernel network for partial differential equations. *arXiv preprint arXiv:2003.03485*, 2020b.
- Zongyi Li, Nikola Kovachki, Kamyar Azizzadenesheli, Burigede Liu, Andrew Stuart, Kaushik Bhattacharya, and Anima Anandkumar. Multipole graph neural operator for parametric partial differential equations. *Advances in Neural Information Processing Systems*, 33:6755–6766, 2020c.
- Zongyi Li, Nikola Kovachki, Chris Choy, Boyi Li, Jean Kossaifi, Shourya Otta, Mohammad Amin Nabian, Maximilian Stadler, Christian Hundt, Kamyar Azizzadenesheli, et al. Geometry-informed neural operator for large-scale 3d pdes. *Advances in Neural Information Processing Systems*, 36, 2024b.
- Rosanne Liu, Joel Lehman, Piero Molino, Felipe Petroski Such, Eric Frank, Alex Sergeev, and Jason Yosinski. An intriguing failing of convolutional neural networks and the coordconv solution. *Advances in neural information processing systems*, 31, 2018.
- Ze Liu, Yutong Lin, Yue Cao, Han Hu, Yixuan Wei, Zheng Zhang, Stephen Lin, and Baining Guo. Swin transformer: Hierarchical vision transformer using shifted windows. In *Proceedings of the IEEE/CVF international conference on computer vision*, pp. 10012–10022, 2021.
- Miguel Liu-Schiaffini, Julius Berner, Boris Bonev, Thorsten Kurth, Kamyar Azizzadenesheli, and Anima Anandkumar. Neural operators with localized integral and differential kernels. *arXiv preprint arXiv:2402.16845*, 2024.
- Jonathan Long, Evan Shelhamer, and Trevor Darrell. Fully convolutional networks for semantic segmentation. In *Proceedings of the IEEE conference on computer vision and pattern recognition*, pp. 3431–3440, 2015.
- Raphael Gontijo Lopes, Dong Yin, Ben Poole, Justin Gilmer, and Ekin D Cubuk. Improving robustness without sacrificing accuracy with patch gaussian augmentation. *arXiv preprint arXiv:1906.02611*, 2019.

- Xin Man, Chenghong Zhang, Jin Feng, Changyu Li, and Jie Shao. W-mae: Pre-trained weather model with masked autoencoder for multi-variable weather forecasting. *arXiv preprint arXiv:2304.08754*, 2023.
- Morteza Mardani, Noah Brenowitz, Yair Cohen, Jaideep Pathak, Chieh-Yu Chen, Cheng-Chin Liu, Arash Vahdat, Karthik Kashinath, Jan Kautz, and Mike Pritchard. Residual diffusion modeling for km-scale atmospheric downscaling. *arXiv preprint arXiv:2309.15214*, 2023.
- Michael McCabe, Peter Harrington, Shashank Subramanian, and Jed Brown. Towards stability of autoregressive neural operators. *arXiv preprint arXiv:2306.10619*, 2023.
- Tung Nguyen, Johannes Brandstetter, Ashish Kapoor, Jayesh K Gupta, and Aditya Grover. Climax: A foundation model for weather and climate. *arXiv preprint arXiv:2301.10343*, 2023a.
- Tung Nguyen, Rohan Shah, Hritik Bansal, Troy Arcomano, Sandeep Madireddy, Romit Maulik, Veerabhadra Kotamarthi, Ian Foster, and Aditya Grover. Scaling transformer neural networks for skillful and reliable medium-range weather forecasting. *arXiv preprint arXiv:2312.03876*, 2023b.
- Adam Paszke, Sam Gross, Francisco Massa, Adam Lerer, James Bradbury, Gregory Chanan, Trevor Killeen, Zeming Lin, Natalia Gimelshein, Luca Antiga, et al. Pytorch: An imperative style, high-performance deep learning library. *Advances in neural information processing systems*, 32, 2019.
- Jaideep Pathak, Shashank Subramanian, Peter Harrington, Sanjeev Raja, Ashesh Chattopadhyay, Morteza Mardani, Thorsten Kurth, David Hall, Zongyi Li, Kamyar Azizzadenesheli, et al. Fourcast-net: A global data-driven high-resolution weather model using adaptive fourier neural operators. *arXiv preprint arXiv:2202.11214*, 2022.
- Ken Perlin. Improving noise. In *Proceedings of the 29th annual conference on Computer graphics and interactive techniques*, pp. 681–682, 2002.
- Olivier Petit, Nicolas Thome, Clement Rambour, Loic Themyr, Toby Collins, and Luc Soler. U-net transformer: Self and cross attention for medical image segmentation. In *Machine Learning in Medical Imaging: 12th International Workshop, MLMI 2021, Held in Conjunction with MICCAI 2021, Strasbourg, France, September 27, 2021, Proceedings 12*, pp. 267–276. Springer, 2021.
- Ilan Price, Alvaro Sanchez-Gonzalez, Ferran Alet, Timo Ewalds, Andrew El-Kadi, Jacklynn Stott, Shakir Mohamed, Peter Battaglia, Remi Lam, and Matthew Willson. Gencast: Diffusion-based ensemble forecasting for medium-range weather. *arXiv preprint arXiv:2312.15796*, 2023.
- Xuebin Qin, Hang Dai, Xiaobin Hu, Deng-Ping Fan, Ling Shao, and Luc Van Gool. Highly accurate dichotomous image segmentation. In *ECCV*, 2022.
- Stephan Rasp and Nils Thuerey. Data-driven medium-range weather prediction with a resnet pretrained on climate simulations: A new model for weatherbench. *Journal of Advances in Modeling Earth Systems*, 13(2):e2020MS002405, 2021.
- Stephan Rasp, Peter D Dueben, Sebastian Scher, Jonathan A Weyn, Soukayna Mouatadid, and Nils Thuerey. Weatherbench: a benchmark data set for data-driven weather forecasting. *Journal of Advances in Modeling Earth Systems*, 12(11):e2020MS002203, 2020.

- Stephan Rasp, Stephan Hoyer, Alexander Merose, Ian Langmore, Peter Battaglia, Tyler Russel, Alvaro Sanchez-Gonzalez, Vivian Yang, Rob Carver, Shreya Agrawal, Matthew Chantry, Zied Ben Bouallegue, Peter Dueben, Carla Bromberg, Jared Sisk, Luke Barrington, Aaron Bell, and Fei Sha. Weatherbench 2: A benchmark for the next generation of data-driven global weather models, 2023.
- Olaf Ronneberger, Philipp Fischer, and Thomas Brox. U-net: Convolutional networks for biomedical image segmentation. In *Medical image computing and computer-assisted intervention–MICCAI 2015: 18th international conference, Munich, Germany, October 5–9, 2015, proceedings, part III 18*, pp. 234–241. Springer, 2015.
- Nitish Srivastava, Geoffrey Hinton, Alex Krizhevsky, Ilya Sutskever, and Ruslan Salakhutdinov. Dropout: a simple way to prevent neural networks from overfitting. *The journal of machine learning research*, 15(1):1929–1958, 2014.
- Richard S Sutton. Reinforcement learning: An introduction. *A Bradford Book*, 2018.
- Ashish Vaswani, Noam Shazeer, Niki Parmar, Jakob Uszkoreit, Llion Jones, Aidan N Gomez, Łukasz Kaiser, and Illia Polosukhin. Attention is all you need. *Advances in neural information processing systems*, 30, 2017.
- Anna Vaughan, Stratis Markou, Will Tebbutt, James Requeima, Wessel P Bruinsma, Tom R Andersson, Michael Herzog, Nicholas D Lane, J Scott Hosking, and Richard E Turner. Aardvark weather: end-to-end data-driven weather forecasting. *arXiv preprint arXiv:2404.00411*, 2024.
- Peng-Shuai Wang. Octformer: Octree-based transformers for 3d point clouds. *ACM Transactions on Graphics (TOG)*, 42(4):1–11, 2023.
- Jonathan A Weyn, Dale R Durran, and Rich Caruana. Improving data-driven global weather prediction using deep convolutional neural networks on a cubed sphere. *Journal of Advances in Modeling Earth Systems*, 12(9):e2020MS002109, 2020.
- Xiaoyang Wu, Li Jiang, Peng-Shuai Wang, Zhijian Liu, Xihui Liu, Yu Qiao, Wanli Ouyang, Tong He, and Hengshuang Zhao. Point transformer v3: Simpler, faster, stronger. *arXiv preprint arXiv:2312.10035*, 2023.
- Enze Xie, Wenhai Wang, Zhiding Yu, Anima Anandkumar, Jose M Alvarez, and Ping Luo. Segformer: Simple and efficient design for semantic segmentation with transformers. *Advances in neural information processing systems*, 34:12077–12090, 2021.
- Sergey Zagoruyko and Nikos Komodakis. Wide residual networks. *arXiv preprint arXiv:1605.07146*, 2016.
- Sixiao Zheng, Jiachen Lu, Hengshuang Zhao, Xiatian Zhu, Zekun Luo, Yabiao Wang, Yanwei Fu, Jianfeng Feng, Tao Xiang, Philip HS Torr, et al. Rethinking semantic segmentation from a sequence-to-sequence perspective with transformers. In *Proceedings of the IEEE/CVF conference on computer vision and pattern recognition*, pp. 6881–6890, 2021.

## A Hyperparameters

In this section, we list all the architecture-specific hyperparameters. See Section 3 in the main paper for information regarding training hyperparameters that were consistent across architectures.

For FNO (Li et al., 2020a), SFNO (Bonev et al., 2023), and UNO (Ashiqur Rahman et al., 2022), we use base modes to be (237, 238). We used domain padding 0.25, the number of layers was 8, and the number of hidden channels was 64 as per our UNet (Ronneberger et al., 2015) configuration.